Journal of Photochemistry & Photobiology, A: Chemistry 453 (2024) 115654

Contents lists available at ScienceDirect

Journal of Photochemistry & Photobiology, A: Chemistry

journal homepage: www.elsevier.com/locate/jphotochem

Investigating the activity of modified TiO_2 photocatalysts used for the photoreforming of biomass derivatives

Muhammad Umair [a], Vittorio Loddo [a,*], Leonardo Palmisano [a], Albin Pintar [b], Gregor Žerjav [b], Giovanni Palmisano [c,d], Samar Al Jitan [c,d], Marianna Bellardita [a,*]

[a] Engineering Department, University of Palermo, Viale delle Scienze Ed. 6, Palermo 90128, Italy
[b] Department of Inorganic Chemistry and Technology, National Institute of Chemistry, Hajdrihova 19, SI-1001 Ljubljana, Slovenia
[c] Department of Chemical Engineering, Khalifa University of Science and Technology, P.O. Box 127788 Abu Dhabi, United Arab Emirates
[d] Research and Innovation Center on CO_2 and H_2, Khalifa University of Science and Technology, P.O. Box 127788 Abu Dhabi, United Arab Emirates

ARTICLE INFO

Keywords:
Photocatalytic H_2 production
Biomass valorisation
Modified TiO_2
Glucose and fructose partial oxidation

ABSTRACT

Different TiO_2 modified (with Pt, Cu_2O, Nb) photocatalysts have been compared for the photo-reforming of glucose and fructose at ambient conditions with the aim of linking the photoactivity to some structural and surface characteristics. A different degree of conversion, distribution of intermediates and H_2 production were observed with the various photocatalysts. Moreover, the results obtained with the same catalysts were slightly different with the two substrates, highlighting the importance of the interaction between the catalyst surface and the organic compound. Bare TiO_2 was inactive towards H_2 production, Cu_2O was effective in replacing Pt for hydrogen generation, and the presence of Pt/Nb was beneficial for both H_2 production and selective oxidation. Moreover, Pt not only works as a sink for the photoproduced electrons, as it is well known in the literature, but also modifies the surface acid-base properties of catalysts as revealed by DRIFT and TPD measurements.

1. Introduction

The traditional industrial processes involving the consumption of fossil fuels have a great impact on global warming and environmental pollution [1]. Therefore, the development of new, eco-friendly and clean industrial processes based on the use of renewable energy has emerged as the most pressing challenge for researchers working in the green chemistry field [2]. The transformation of biomass into chemicals is a promising approach to counter the negative impacts caused by the excessive consumption of fossil fuels [3,4]. Natural biomass is a renewable energy source that does not emit greenhouse gases because it is created by plants during photosynthesis from CO_2 and water [5]. Biomass and its derivatives are considered valuable inexpensive raw materials for pharmaceutical, food, cosmetic and fuel industry [5–8]. Furthermore, hydrogen production from biomass is considered a valid alternative to traditional expensive methods. Hydrogen is a clean, affordable, efficient, inexhaustible, storable, and eco- friendly fuel that produces just water when burned, with no pollutants, particulates or greenhouse gases released into the atmosphere [9–11]. Glucose and fructose, which derive from cellulose, can be used to produce high-value compounds in a sustainable mode. In particular, they can be used to make ethanol, mannitol and sorbitol through hydrogenation, 5-hydroxymethyl furfural through dehydration, gluconic acid, arabinose and erythrose by partial oxidation and hydrogen [12–19].

Photocatalysis is an environmentally friendly process used in organic synthesis and pollutant removal [3,20–23]. The use of photocatalysis has several advantages for the environment, including mild operating conditions (i.e. room temperature and ambient pressure), the absence of harmful chemical solvents, the possibility of solar light utilization as irradiation source, the easy integration with other physical and chemical technologies, e.g. membrane separation [24–26].

Titanium dioxide is the most studied photocatalyst and considered highly desirable because of its low cost, non-toxicity, low environmental impact, significant oxidizing power, outstanding photocatalytic activity, and long-term (photo)stability [27–29]. However, it presents some disadvantages. Because of large band energy, it can only be activated by UV light and the fast recombination rate of the photoexcited electron-hole pairs makes its use not very effective. To address this issue, different strategies can be pursued [29–32]. The treatment by ultrasound was effective in forming oxygen vacancies which allow activation

* Corresponding authors.
E-mail addresses: vittorio.loddo@unipa.it (V. Loddo), marianna.bellardita@unipa.it (M. Bellardita).

https://doi.org/10.1016/j.jphotochem.2024.115654
Received 19 February 2024; Received in revised form 9 March 2024; Accepted 31 March 2024
Available online 1 April 2024

under visible light [33,34]; the coupling of TiO_2 with other suitable semiconductor materials can improve the solar light absorption, enhance the photocatalytic activity and change the surface acidity [35–39]. Moreover, the doping with metals (i.e., Nb, Cu, Co, Ni, Au) has been reported to be effective in the reduction of the recombination rate of photoexcited electron-hole pairs and modification of some surface features [26,39–47]. Cu_2O-based materials are used for a broad range of applications, such as sensing, disinfection, desulfurization, organic synthesis, photovoltaics, photodegradation, and photocatalysis. TiO_2 is a widely studied n-type semiconductor, whereas Cu_2O is a typical p-type semiconductor with a low band gap of 2.2 eV. They might come together to form a p-n heterojunction, which can absorb solar spectrum radiation, boost photogenerated charge carrier separation, and increase photocatalytic performances [48–51]. Notably, by considering the energetic level of Cu_2O conduction band edge, the hydrogen production can be boosted [36,52,53].

TiO_2 exists in three main crystalline phases, i.e. rutile, anatase and brookite that exhibit different photocatalytic activity [54–58]. Brookite, the relative new polymorph [54], has shown to be active towards the partial oxidation of glucose and towards the formation of hydrogen [59,60].

Platinum (Pt), on the other hand, was widely used in photoreforming reactions due to its largest work function (5.65 eV), higher stability with respect to other metals and the lowest over potential for H_2 formation [33,60–62]. In recent years, the efforts of the scientific community have turned to the search for ecological and economic alternatives to noble metals and Cu_2O has received wide acclaim [36,63,64]. Moreover, the design of Pt and Cu modified catalysts in the form of single-site metal atoms or clusters, allowed the presence of high amounts of active sites, thus enhancing the catalytic activity [65,66].

In this work, TiO_2-based photocatalysts (anatase, rutile and brookite) modified by Pt loading, Nb doping and coupled with Cu_2O were prepared to highlight that the intrinsic characteristics of the TiO_2 polymorphs can influence the distribution of foreign species. The photoactivity of the different powders was compared towards glucose and fructose reforming, used as probe molecules of biomass derivatives. Slightly different synthesis procedures were used to prepare the polymorphic forms of TiO_2. The surface and the chemical-physical properties of synthesized catalysts have been thoroughly studied with the aim of correlating the photoactivity to some features of the solids and highlight the role of Pt, that is worldwide used only as electrons sink. Notably, it was found that the noble metal had an important unusual role to modify the surface acid-base properties of the photocatalysts as indicated by DRIFTS and TPD characterizations.

2. Experimental

2.1. Chemicals

Ethanol (C_2H_5OH), titanium tetrachloride 98 % ($TiCl_4$), hydrochloric acid 37 % (HCl), titanium(IV) isopropoxide $\geq$ 97 % ($Ti(OCH(CH_3)_2)_4$) named as TIP, Pluronic P127, copper(I) chloride (CuCl), niobium(V) chloride ($NbCl_5$), copper(I) oxide (Cu_2O) and platinum chloride ($PtCl_4$) were purchased from Sigma-Aldrich and used without further purification for the synthesis of different photocatalysts. Commercial samples of BDH (anatase) and P25 (anatase + rutile) were also used as reference materials and for the purpose of comparison.

2.2. Catalysts preparation

2.2.1. Brookite

Brookite was prepared through hydrothermal hydrolysis. 210 mL of distilled water, 80 mL of HCl (concentrated) and 5 mL of $TiCl_4$ were added in a 500 mL beaker under stirring. After ca. 2 h the mixture was shifted into a Pyrex bottle and heated at 373 K in an oven for 48 h. The resulting combination powder was a mixture of brookite and rutile. By peptizing with water at different times, pure brookite nanoparticles were recovered in the supernatant and rutile phase was present as a precipitate. This sample was identified as Brookite.

Niobium (Nb) loading was accomplished by adding $NbCl_5$ to the solution obtained by dissolution of $TiCl_4$. Nb1-brookite was the code used for this sample where 1 % indicates the nominal weight percentage of Nb with respect to TiO_2. Nb was chosen both because it is reported to enhance the photoactivity of TiO_2 [26,67] and to modify its surface acid properties [68].

2.2.2. Home prepared TiO_2 (HP)

The sample indicated as HP was prepared by adding titanium(IV) isopropoxide (TIP) to an aqueous solution containing HCl, Pluronic P127 and C_2H_5OH. The following molar ratios were used: TIP (1): H_2O (15): C_2H_5OH (40): HCl (0.5): P127 (0.005). The resulting dispersion was mixed for approximately 4 h at room temperature and then heated overnight at 383 K. The recovered solid was calcined for 24 h at 773 K.

2.2.3. Cu_2O-TiO_2 samples

Some Cu_2O (3 wt%)-TiO_2 coupled samples were prepared by mixing the two oxides by a Retsch Ball Mills, type PM100 ball milling. The powders were mixed for 2 h at 150 rpm, reversing the sense of the rotation after 1 h and 10 min of pause. The Cu_2O percentage was chosen considering the results obtained in a previous paper [36].

2.2.4. Pt-loaded samples

Some TiO_2 catalysts were loaded with 0.5 wt% Pt by a photodeposition method. Distilled water (200 mL), ethanol (50 mL), $PtCl_4$ (5 mL) and TiO_2 based sample (1 g) were added in a photoreactor. The obtained mixture was stirred in the dark for 0.5 h with He (or N_2) bubbling, and then illuminated with a UV lamp (125 W) for 7 h. The resulting mixture was filtered, washed thoroughly with distilled water and then dried in an oven for 6 h.

2.3. Catalysts characterization

X-ray diffraction (XRD) patterns of the investigated powders were obtained by a Philips diffractometer (operative at a current of 30 mA and a voltage of 40 kV) using the CuKα radiation. The phase composition of some samples has been calculated in accordance with Zhang and Banfield [69] while the crystallinity degree has been determined according to the method reported by Bellardita et. al. [70,71].

The morphology was examined by scanning electron microscopy (SEM) using a Nova NanoSEM instrument. A small amount of powder samples was placed on carbon tape attached to a stainless-steel stub. Transmission electron microscopy (TEM) was performed using a Titan transmission electron microscope operating at 300 kV. The samples were prepared by suspending the powder in 2-propanol, treating with ultrasound, and finally depositing 3 μL of the suspension 2 consecutive times on a 400-mesh Au grid provided by Tedpella. The solvent was then evaporated at room temperature. ImageJ was used to evaluate the lattice d-spacing and the size of the nanoparticles. The specific surface areas (SSA) were determined in a Flow Sorb 2300 apparatus (Micromeritics) by using the single-point BET method.

Zeta potential measurements were performed using a Malvern Panalytical Zetasizer Ultra Red instrument equipped with a Malvern Multipurpose Titrator MPT-3. 25 mg of a photocatalyst was dispersed in 100 mL of ultrapure water and stirred for 30 min (400 rpm). 0.25 M and 0.025 M hydrochloric acid and 0.25 M sodium hydroxide were used to adjust the pH in the measurement range.

The UV–Vis diffuse reflectance spectra (DRS) were acquired in the wavelength range of 200–800 nm at room temperature by using a Shimadzu UV-2401 PC spectrophotometer with barium sulphate ($BaSO_4$) as the reference material. Band gap values were calculated by plotting the modified Kubelka-Munk function, $[F(R'_\infty)hv]^{½}$ against the energy of the stimulating light. The solid-state photoluminescence spectra (PL) of the

investigated photocatalysts were recorded with a Perkin Elmer UV–Vis fluorescence spectrometer LS 55 in the range of 300–600 nm at an excitation wavelength of 300 nm. Raman spectra of the photocatalysts were obtained by means of a BWTek-i-micro Raman Plus System, equipped with a 785 nm diode laser.

X-ray photoelectron spectroscopy (XPS) was performed using a Thermo Fisher Scientific (TFS) Escalab Xi + XPS with an AlKα X-ray source. Prior to the XPS measurements, the samples were etched *in situ* with an Ar beam to remove contaminants from the top layer.

For the identification of the free radical species of the catalyst, electron paramagnetic resonance (EPR) was performed on an EMX-nano spectrometer (Bruker Biospin Corp., Karlsruhe, Germany). For the detection of transition metals and oxygen vacancies, the powder was placed in a tube and was fitted into the sample holder in the EPR test chamber for analysis. For the detection of superoxide anion radicals ($^{\bullet}O_2^-$) , the sample was dissolved in methanol to form a 1 mg/mL suspension which was then dispersed using ultrasonication. Subsequently, 100 mM of trapping agent 5,5 Dimethyl-1-pyrroline N-oxide (DMPO) was added into the suspension. After stirring, the mixture was placed in a tube and was fitted into the sample holder in the EPR test chamber for analysis. For the detection of hydroxyl radical ($OH^{\bullet}$), the sample was dissolved in water to form a 1 mg/mL suspension which was then dispersed using ultrasonication. Subsequently, 100 mM of trapping agent 5,5 Dimethyl-1-pyrroline N-oxide (DMPO) and 100 μL of 1 mM H_2O_2 were added into the suspension. After stirring, the mixture was placed in a tube and was fitted into the sample holder in the EPR test chamber for analysis. The sample was irradiated for 30 min using a UV (LOT-Quantum Design GmbH) lamp and data were recorded.

The Diffuse Reflectance Infrared Fourier Transform Spectroscopy (DRIFTS) spectra of the studied catalysts after adsorption of pyridine were recorded using a Perkin Elmer Frontier FT-IR spectrometer equipped with a mercury cadmium telluride (MCT) detector. A catalyst sample placed in a DRIFTS cell was first heated in an N_2 stream from room temperature to 473 K and then held at this temperature for 15 min to remove impurities from the catalyst surface. The sample was then cooled to 393 K in an N_2 stream, and a background spectrum was recorded. After saturating the catalyst surface with a pyridine containing N_2 stream for 20 min at 393 K, the catalyst sample was purged with pure N_2 and held at 393 K for additional 2 h to remove the excess pyridine. The FT-IR spectra (an average of 64 scans, resolution of 4 cm^{-1}) were recorded at 393 K.

Surface acidic sites were revealed using pyridine as a probe molecule and a Perkin Elmer Pyris 1 TGA instrument. Samples were first heated from 323 to 473 K and held at this temperature for 15 min to remove contaminants from the catalyst surface. The samples were then cooled to 393 K and pyridine was adsorbed with a saturated N_2 stream until the weight of the catalyst was constant (after about 20 min). The powders were then purged with N_2 and held at 393 K for 2 h to remove excess pyridine. TPD (temperature-programmed desorption) profiles were recorded in the temperature range from 393 to 773 K.

To determine basic properties of the surface of investigated photocatalysts, CO_2 TPD profiles were obtained by heating samples in an O_2 (5 %)/He stream (25 mL/min) from room temperature to 398 K (10 K/min) in the Micromeritics AutoChem II 2920 apparatus. After 10 min, the samples were cooled to 323 K and then the gas flow was changed to Ar (25 mL/min). CO_2 was introduced by dosing CO_2 (80 vol%)/Ar into the Ar stream (25 mL/min) flowing through the samples at 323 K. Desorption of CO_2 from the sample into the Ar stream (25 mL/min) was monitored over the temperature range of 323–633 K (heating ramp 10 K/min) using the Pfeiffer Vacuum ThermoStar mass spectrometer.

2.4. Photocatalytic activity determination

Photocatalytic activity was studied in anaerobic conditions by using separately two substrates, i.e. glucose and fructose, at room temperature and atmospheric pressure, monitoring the evolution of H_2 and CO_2 in the gas phase and the formation of the intermediates in the liquid phase. An 800 mL Pyrex cylindrical reactor was used, and He or N_2 were bubbled into the solution for 30 min to achieve the adsorption–desorption equilibrium of the substrate on the catalysts surface. After that, the reactor was sealed, and the near-UV lamp (125 W medium pressure Hg) was switched on. The initial concentration of the two substrates was 1 mM and the reactions were carried out at a pH of about 5, the "natural" pH of the aqueous suspension of both substrates measured after adding the catalyst. A radiometer was used to check the optimum amount of the photocatalysts able to absorb ca. 90 % of the photons emitted by the lamp. Specific amounts ranging between 0.3 and 0.8 g/L were obtained for the different photocatalysts. To investigate the role of the main active species generated under irradiation in the photocatalytic system, runs in the presence of selected scavengers (1 mM) were done in the presence of glucose and Pt-HP as photocatalyst. Namely, *tert*-butanol was used as $^{\bullet}OH$ scavenger, $AgNO_3$ as electrons scavenger, $Na_2C_2O_4$ as holes scavenger and 1,4-benzoquinone as a $^{\bullet}O_2^-$ scavenger. To determine the substrates' adsorption on the catalyst surface in the absence of light, their concentration values were measured after 30 min of stirring of the suspension containing the catalyst under dark conditions. The experimental setup is shown in Fig. S1. The photocatalytic reactions lasted 5 h and samples were withdrawn periodically during the irradiation time, and filtered by 2 μm membranes (HA, Millipore). A Thermo Scientific Dionex ultimate 3000 HPLC, equipped with a Diode Array and refractive index detectors, was used for the quantitative determination of glucose and fructose and for identifying their reaction products. The eluent was a 2.5 mM H_2SO_4 aqueous solution, the flow rate was 0.6 mL/min and the column was a Phenomenex REZEK ROA H^+ Organic acid H^+. In order to monitor the evolution of the gaseous species during the runs, 500 μL gas were withdrawn at specific time intervals from a valve at the top of reactor. A HP 6890 Series GC System equipped with a Supelco packed column GC 60/80 Carboxen$^{TM\text{-}1000}$ and a thermal conductivity detector (TCD) was used to measure the content of H_2 and CO_2.

3. Results and discussion

Fig. 1 shows the XRD patterns of all prepared photocatalysts. The three main polymorphs (anatase, rutile and brookite) of TiO_2 are indicated as A, R, B, respectively. The commercial TiO_2 BDH consists of only anatase phase, whereas P25 contains both the anatase and rutile phases. HP contains mainly anatase phase and also traces of rutile, pure brookite was home prepared. The commercial samples (P25 and BDH) show more intense and narrow peaks compared to those of the home prepared ones indicating a better crystallinity, due to their preparation at high temperature on industrial scale. Moreover, no diffraction peaks related to foreign species are present, probably due to the high degree of the dispersion and the low amount of these species with respect to TiO_2.

The crystal phase and specific surface area (SSA) of all the samples are listed in Table 1. Commercial samples exhibit lower SSA as compared to that of home prepared photocatalysts, being 48 $m^2 \bullet g^{-1}$ for 3 %Cu_2O-P25 and 69 $m^2 \bullet g^{-1}$ for 3 %Cu_2O-HP, respectively. Brookite samples display higher SSA ranging between 90 and 98 $m^2 \bullet g^{-1}$, whilst Pt-BDH shows the lowest SSA of 10 $m^2 \bullet g^{-1}$. The phase composition and the crystallinity degree of the bare TiO_2 based samples are reported in Table S1. Commercial P25 consists of 78 % of anatase and 22 % of rutile in accordance with literature [70], whilst the home prepared HP contains 69 % of anatase and 31 % of rutile. The home prepared samples are the less crystalline ones due to the low temperature at which they were synthesized. The presence of Pt and of the other species, did not significantly influence both the phase composition and the crystallinity.

SEM images of all prepared samples are displayed in Fig. S2. All samples are formed by aggregates of irregular roundish particles whose size range is 30–130 nm. Due to the lower synthesis temperature, the particle sizes of homemade samples are smaller than those of commercial samples.

Diffuse reflectance spectra (DRS) of the different TiO_2-based samples

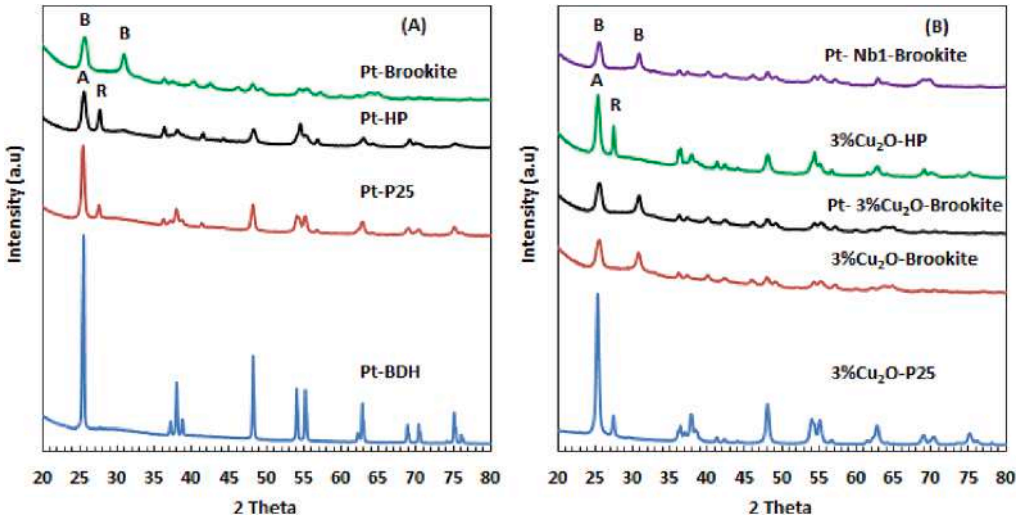

Fig. 1. XRD patterns of: (A) Pt-BDH, Pt-P25, Pt-HP, and Pt-Brookite; (B) 3 %Cu_2O-P25, 3 %Cu_2O-Brookite, Pt-3 % Cu_2O-Brookite, 3 %Cu_2O-HP, and Pt-Nb1-Brookite samples. A = Anatase, B = Brookite, R = Rutile.

Table 1
Some physical–chemical properties of the investigated photocatalysts: composition (A = Anatase, R = Rutile, B = Brookite), band-gap, SSA and TPD results (amount and density of acid sites of catalysts and the corresponding temperatures of pyridine desorption).

Catalyst	Phase	Band gap (eV)	SSA (m^2/g)	Quantity of acid sites (mmol/g)	Density of acid sites (mmol/m^2)	Temperature of pyridine desorption (°C)
BDH	A	3.24	10	0.0095	0.0010	289
Pt-BDH	A	3.26	10	0.0091	0.0009	[a]N.D.
P25	A + R	3.18	50	0.1194	0.0024	289
Pt-P25	A + R	3.09	50	0.0944	0.0019	323, 388
3 %Cu_2O-P25	A + R	3.08	48	0.1253	0.0026	264, 342
Brookite	B	3.34	98	0.2721	0.0028	406
Pt-Brookite	B	3.32	98	0.4836	0.0049	235, 408
Pt-Nb1-Brookite	B	3.27	90	0.2669	0.0030	402
3 %Cu_2O-Brookite	B	3.33	91	0.2237	0.0025	290, 413
Pt-3 %Cu_2O-Brookite	B	3.33	94	0.2669	0.0028	290, 403
HP	A + R	2.96	78	0.1605	0.0021	310
Pt-HP	A + R	3.01	78	0.1137	0.0015	375
3 %Cu_2O-HP	A + R	3.05	69	0.1537	0.0022	261, 350
Cu_2O	Cu_2O	1.97	1	0.0009	0.0009	428

[a] N.D.: Not determined because no pyridine desorption peak was observed in the measured temperature range (see Fig. S8).

are shown in Fig. S3. All the photocatalysts absorb light in the UV–visible range. The BDH and Brookite samples (Fig. S3A) show an absorption band in the high energy region ($\lambda < 360$ nm), whilst all other samples exhibit a slight shift in absorption towards longer wavelengths. Pt presence and copper loading (Fig. S3B) enhance the absorption at $\lambda >$ 420 nm and slightly shift the absorption edge towards the visible part of spectrum.

Band gap values of all samples, measured by plotting the modified Kubelka-Munk function, $[F(R'_\infty)h\nu]^{½}$ against the energy of the stimulating light, are reported in Table 1. All the powders exhibit band gap values in the range of 2.96–3.33 eV being the lowest value found for HP and highest figures observed for brookite based samples. No relevant variation with respect to pristine TiO_2 samples were observed in the presence of foreign species.

Fig. S4 shows the Raman spectra of TiO_2 based composites. Raman bands at 144 cm^{-1} (E_g), 197 cm^{-1} (E_g), 396 cm^{-1} (B_{1g}), 514 cm^{-1} (A_{1g}), and 637 cm^{-1} (B_{1g}) are characteristic of anatase phase, whilst those at 446 cm^{-1} and 613 cm^{-1} are related to the rutile one. In P25 and HP based samples, being anatase the main component, the presence of rutile can be detected by enlarging the figures while there are no peaks relating to Cu_2O due to probably its small amount and dispersion within the TiO_2 matrix. In Fig. S4B the bands at 126 cm^{-1}, 152 cm^{-1}, 212 cm^{-1}, 247 cm^{-1}, 322 cm^{-1}, 364 cm^{-1}, 409 cm^{-1}, 456 cm^{-1}, 498 cm^{-1}, 543 cm^{-1}, 582 cm^{-1} and 632 cm^{-1} are characteristic of brookite. In brookite-containing samples, the addition of the metal caused a decrease of the band intensity that can be attributed to the greater surface disorder due to the presence of Pt on the TiO_2 surface. There were no identifiable peaks of Pt, and this is consistent with the observation that this metal is not present within the TiO_2 lattice but only on the surface. Also in this case no Cu_2O peaks were detectable.

Fig. 2 displays the zeta potential versus pH curves of some Pt-TiO_2 samples. The IEP (isoelectric point, i.e. the pH value at which the net charge on the catalyst surface is zero) values are 4.23 for Pt-BDH, 4.45 for Pt-HP, 5.00 for Pt-P25 and 5.63 for Pt-Brookite. The above findings imply that at pH 5 (pH at which the photocatalytic runs were carried out) the catalyst's surface is negatively charged for Pt-BDH and Pt-HP, neutral for Pt-P25 and positively charged for Pt-Brookite. Then different coulombic interactions can take place between the species in the reaction mixture and the surface of the various TiO_2 powders [72].

The presence of noble metals such as Pt has been reported to be effective for the visible-light activation and the enhancement of the TiO_2 performance [73]. In fact, the Fermi levels of noble metals are lower than that of TiO_2, and this results in the transfer of the photogenerated electrons from the conduction band of TiO_2 to metal particles [74]. This process reduces the electron–hole recombination rate as can be seen from the decrease of the intensity of the photoluminescence bands in the presence of Pt (Fig. 3) [75]. For all the samples, except for BDH which displays a peak at 380 nm, the main emission bands are at ca. 423 nm

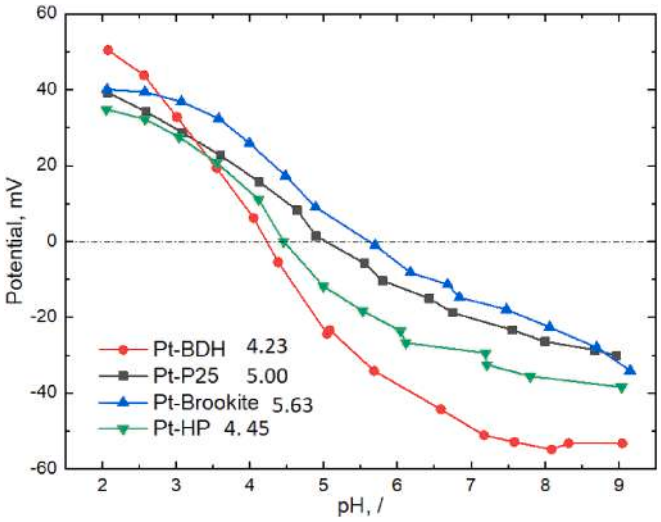

Fig. 2. Results of the pH-related zeta potential measurements.

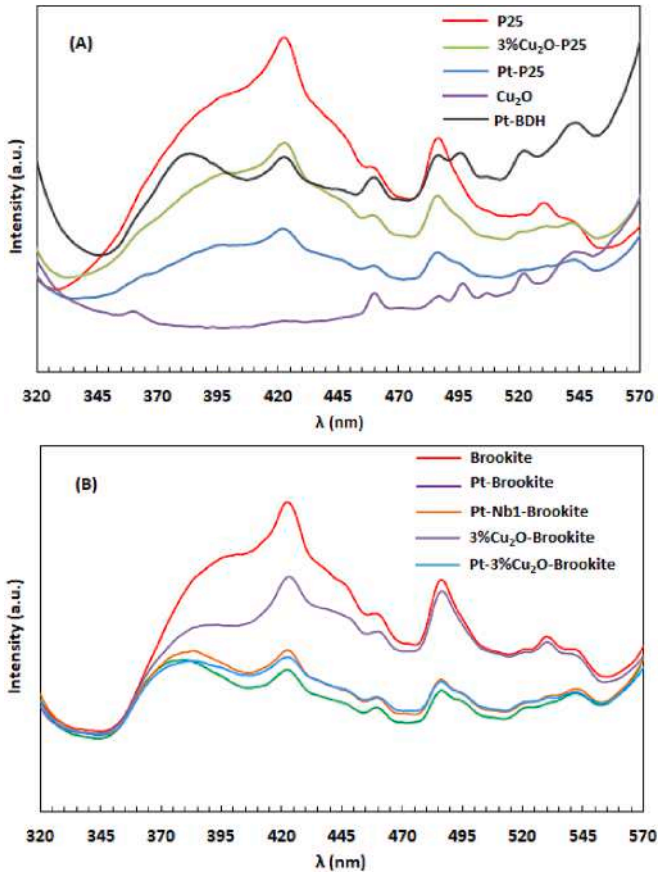

Fig. 3. Photoluminescence spectra of the different samples.

and this can be attributed to the band-to-band indirect transition of electrons in TiO_2 in accordance with the band gap values. The signals at higher wavelength can be assigned to a non-radiative recombination of the excited electrons towards lattice defects [53,76]. A significant decrease in the PL intensity can be noticed after the coupling with Cu_2O and the addition of Nb due to the lower recombination rate of the photogenerated charges [36].

TEM images of the different samples were acquired to investigate the morphology, the particles dimension, and the distribution of the different components. Some selected images are reported in Fig. 4, images of other samples are given in the Supporting Information (Fig. S5). TEM images of the sample Pt-P25 (Fig. 4A) reveal that Pt nanoparticles (represented by small dark spheres) are uniformly dispersed across the P25 surface confirming the effectiveness of the photodeposition method. The size of Pt nanoparticles is approximately 2 to 3 nm while the size of P25 particles (anatase and rutile) ranges between 10 and 20 nm. By zooming in on the image, it is possible to distinguish two lattice fringes of ca. 0.35 nm and 0.32 nm, characteristic of the (1 0 1) anatase and (1 1 0) rutile planes, respectively [77]. SAED (selected-area electron diffraction) patterns consisting of concentric rings indexed as the various planes of rutile and anatase, confirmed the biphasic structure of P25. In the HP sample (Fig. 4B), instead, Pt nanoparticles are clustered into one area on the TiO_2 surface. The size of TiO_2 particles ranges between 5 and 25 nm, which is slightly larger range compared to the Pt-P25 sample, and the size of Pt nanoparticles is ca. 1 to 2 nm that is slightly smaller than found in the Pt-P25 sample. Also, in this case an intimate contact between anatase and rutile can be observed. Brookite consists of rod-shaped particles which size ranges between 10 and 30 nm (Fig. 4C). Pt nanoparticles (dimensions ca. 2–3 nm) are concentrated in some areas whilst Nb particles are not distinguishable due to their low quantity and high degree of dispersion in the TiO_2 matrix. The different distribution and size of Pt nanoparticles on the surface of the different TiO_2 based samples can be attributed to some specific physical–chemical properties of the samples as specific surface area, surface acidity/basicity, hydroxylation degree [78], hydrophilicity [79], ability to adsorb water [80] which can also induce the formation of oxidized species of Pt.

In the Cu_2O/TiO_2 composite samples a good contact between the two components can be clearly seen in the images reported in Fig. S5. The sizes of Cu_2O particles range between 5 and 10 nm, which are smaller than those of TiO_2 particles.

XPS measurements of some selected samples were carried out to examine the surface composition and the oxidation states of the different species. In Fig. S6 the XPS survey spectrum of the samples with the various species indicated is presented. Peaks for Pt (not shown in XPS survey) were barely detected due to its small atomic concentration. Cl, as residual species deriving from $TiCl_4$, $PtCl_4$ and $NbCl_5$ precursors, was also detected. When both present, Cl and Nb are not clearly distinguishable because their peaks almost overlap. In Fig. 5A are reported the high resolution XPS spectra of the Ti 2p peaks. In Pt-P25 sample the two peaks of Ti $2p_{3/2}$ at 459.5 eV and Ti $2p_{1/2}$ at 465.3 eV with a binding energy distance of 5.8 eV are characteristic of Ti^{4+} in TiO_2 [81]. The Ti $2p_{3/2}$ shoulder peak at 461.4 eV which is visible only for the 3 %Cu_2O-P25 sample is characteristic of Ti^{3+}. This indicates that in this sample Ti is present in two oxidation states (+3 and + 4) due to an electron transfer from Cu_2O to P25. The high-resolution O 1s spectra are shown in Fig. 5B. For almost all of the samples the main peak is that at ca. 530.7 eV, assigned to O^{2-} ions of the TiO_2 crystalline lattice. The peak at ca. 533.0 eV, related to –OH groups [82], is weak in Pt-Nb1-Brookite, Pt-HP and Pt-P25, but more evident in 3 %Cu_2O-P25 and 3 %Cu_2O-HP. The presence of Cu_2O seems to favour the formation of surface hydroxyl groups and for the 3 %Cu_2O-HP sample the adsorption of H_2O. Cu_2O on the TiO_2 surface may introduce new active sites or modify existing ones, affecting the adsorption behaviour of molecules, including water. The main Pt peak at ca. 76 eV (Fig. 5C) corresponds to Pt^0, the less intense peaks are characteristic of partially oxidized Pt species [83].

High resolution XPS spectra of Cu 2p are reported in Fig. 5D. For the P25 sample, the binding energy of the Cu $2p_{1/2}$ peak at 955.4 eV and of $2p_{3/2}$ at 933.2 eV are characteristic of Cu(I) oxide. For the HP sample the presence of a shakeup satellite peak between the main two Cu 2p peaks is characteristic of Cu^{2+} ions. The difference in Cu states between the P25 sample and HP could be the reason why water adsorption seems to be favoured only on the HP sample. In other words, Cu(I) oxide on the P25 surface may not provide favourable sites for water adsorption compared to Cu^{2+} ions on the HP surface. The higher oxidation state in the HP sample could lead to a different surface structure or electronic

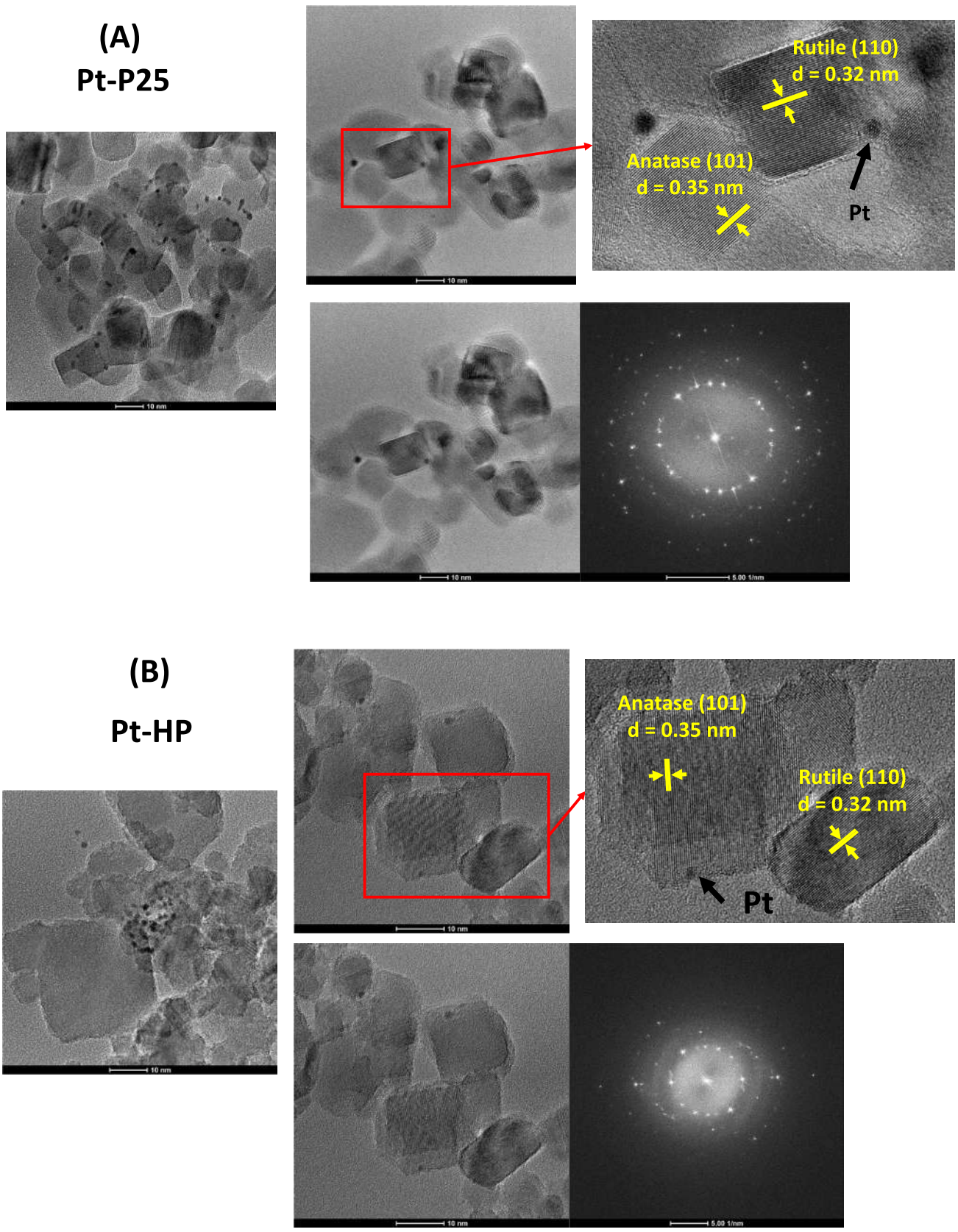

Fig. 4. TEM images of the samples: (A) Pt-P25, (B) Pt-HP, and (C) Pt-NB1-Brookite.

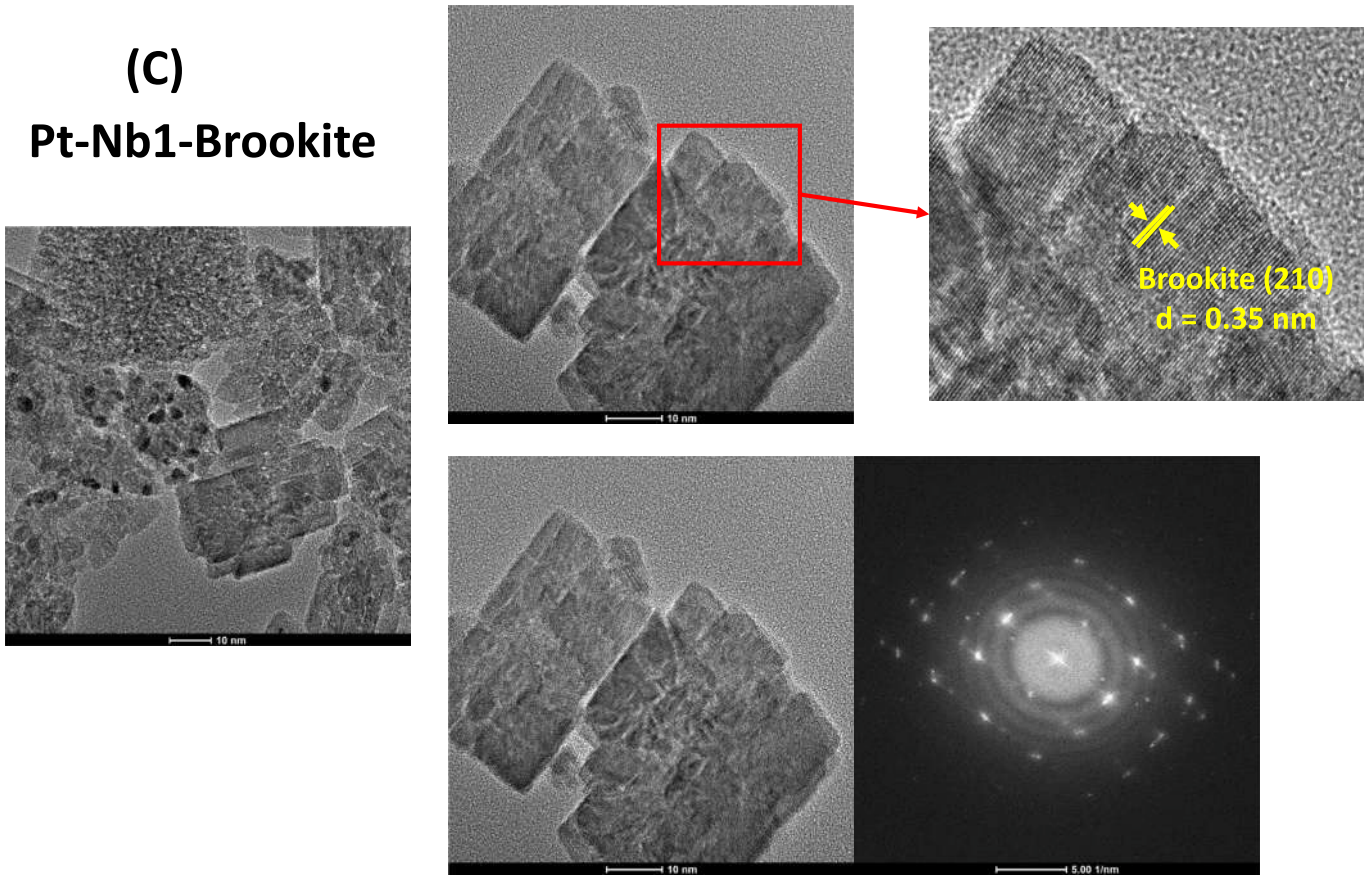

Fig. 4. (*continued*).

configuration that enhances water adsorption.

The Nb 3d spectrum (Fig. 5E) displays two peaks at 209.9 eV and 207.1 eV (binding energy distance of 2.8 eV) characteristic of Nb_2O_5 [84]. The other two peaks at lower binding energies are those of Cl 2p.

In Table S2 the atomic concentrations of the different species obtained by XPS investigations are reported.

As illustrated in Fig. S7, the EPR spectra of the powder samples 3 % Cu_2O-P25, 3 %Cu_2O-HP and Pt-3 %Cu_2O-Brookite show a broad signal at g = 1.999 which can be assigned to Ti^{3+} ions on the surface [85]. The experiments carried out with samples containing Nb did not show any EPR signal, pointing out that the photocatalysts are unable to generate free electrons and oxygen vacancies under illumination. The Pt-3 % Cu_2O-Brookite sample shows the highest intensity peaks indicating stronger presence of free electrons and oxygen vacancies, probably because the electrons are transferred to Pt and trapped therein. Conversely, the 3 %Cu_2O-P25 solid showed the lowest EPR peak intensity. In the presence of DMPO/MeOH solutions (Fig. 6), the experiments carried out in the dark cannot detect any EPR signal, indicating that the photocatalysts are unable to generate radicals in absence of illumination. When the photocatalysts get exposed to light, the EPR spectra give rise to the characteristic paramagnetic resonance absorption of the adducts of DMPO-$^{\bullet}O_2^-$. This result indicates that all the photocatalysts can thermodynamically produce superoxide anion radicals ($^{\bullet}O_2^-$) under illumination.

For DMPO/H_2O_2/water suspended samples (Fig. 7), in the dark, no EPR signal is detected. Under irradiation, the EPR spectra give rise to the characteristic paramagnetic resonance absorption of the adducts of DMPO-$^{\bullet}$OH. Results indicate that only 3 %Cu_2O-P25 and 3 %Cu_2O-HP samples can thermodynamically produce hydroxyl ($^{\bullet}$OH) radicals under illumination. Samples with brookite phase TiO_2 were unable to produce $^{\bullet}$OH radicals under light. While brookite TiO_2 can still exhibit some photocatalytic activity, it's often less efficient in generating hydroxyl radicals under light compared to anatase and rutile. This is due to the variations in electronic structure, band gap, and surface properties among the different TiO_2 phases. The P25 sample showed the highest intensity peaks indicating strongest formation of the hydroxyl radicals.

In situ DRIFTS of adsorbed pyridine was used to identify the nature and the density of surface acid sites. In Fig. 8 are illustrated the spectra related to bare and different Pt-loaded TiO_2 samples. The peaks at 1445 cm^{-1}, 1486 cm^{-1}, 1574 cm^{-1} and 1604 cm^{-1} are related to the pyridine ring coordinated to surface Lewis acid sites, whilst those at 1545 cm^{-1} and 1635 cm^{-1} correspond to the Brønsted acid sites on which the pyridinium ions are adsorbed [86–90]. A clear predominance of acidic Lewis sites is detectable in all samples; in addition, these spectra show the presence of both protonated pyridine (1545 and 1635 cm^{-1}) and coordinated pyridine (at 1604 and 1445 cm^{-1}). The peak at 1574 cm^{-1} is ascribable to a weak interaction of pyridine with the acid sites on the catalyst surface. Sharp and intense peaks are present for commercial P25 and home prepared HP samples, moderate for brookite and very weak for BDH solids. Although these spectra essentially give qualitative information, we can roughly say that a higher intensity corresponds to a higher concentration of acid sites, consequently the BDH sample exhibits the lowest concentration of surface acid sites, while P25 and HP solids the largest. Pt loading causes a decrease in the intensity of the bands for P25 (Fig. 8A) and HP (Fig. 8C) samples, a little increase for BDH solid (Fig. 8B) and a significant rise for Brookite sample (Fig. 8D). The different effects of Pt on the various samples can probably be due to some peculiar features of the diverse TiO_2 phases as different hydrophilicity [80], hydroxylation degree [78] and surface acidity/basicity. IR spectra recorded in the presence of adsorbed CO revealed the presence of different Pt species with a different distribution on the various TiO_2 polymorphs [80]. Shifts to higher wavenumbers of the peaks at

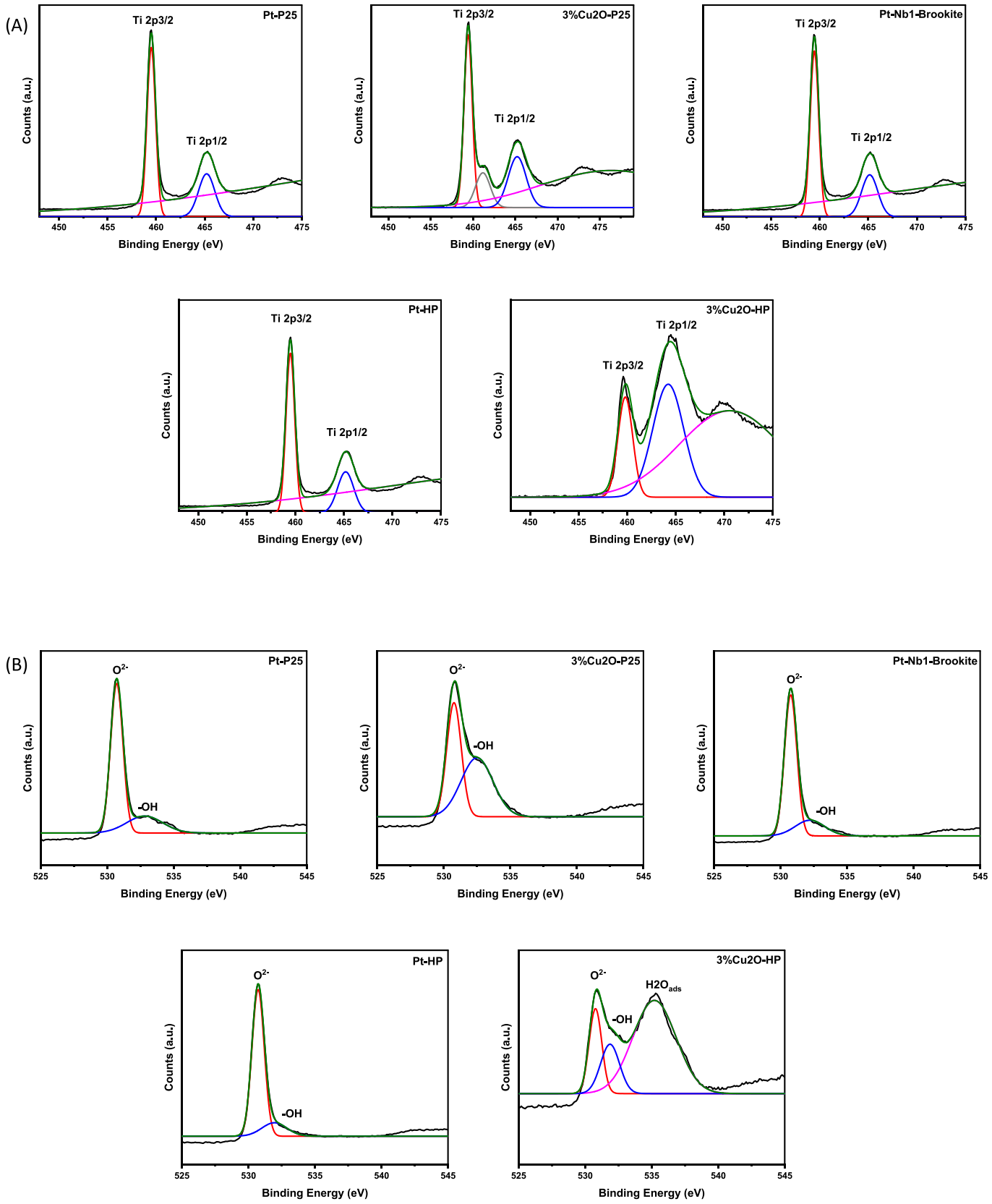

Fig. 5. High resolution XPS spectra with deconvolution of: (A) Ti 2p, (B) O 1s, (C) Pt 4f, (D) Cu 2p, and (E) Nb 3d.

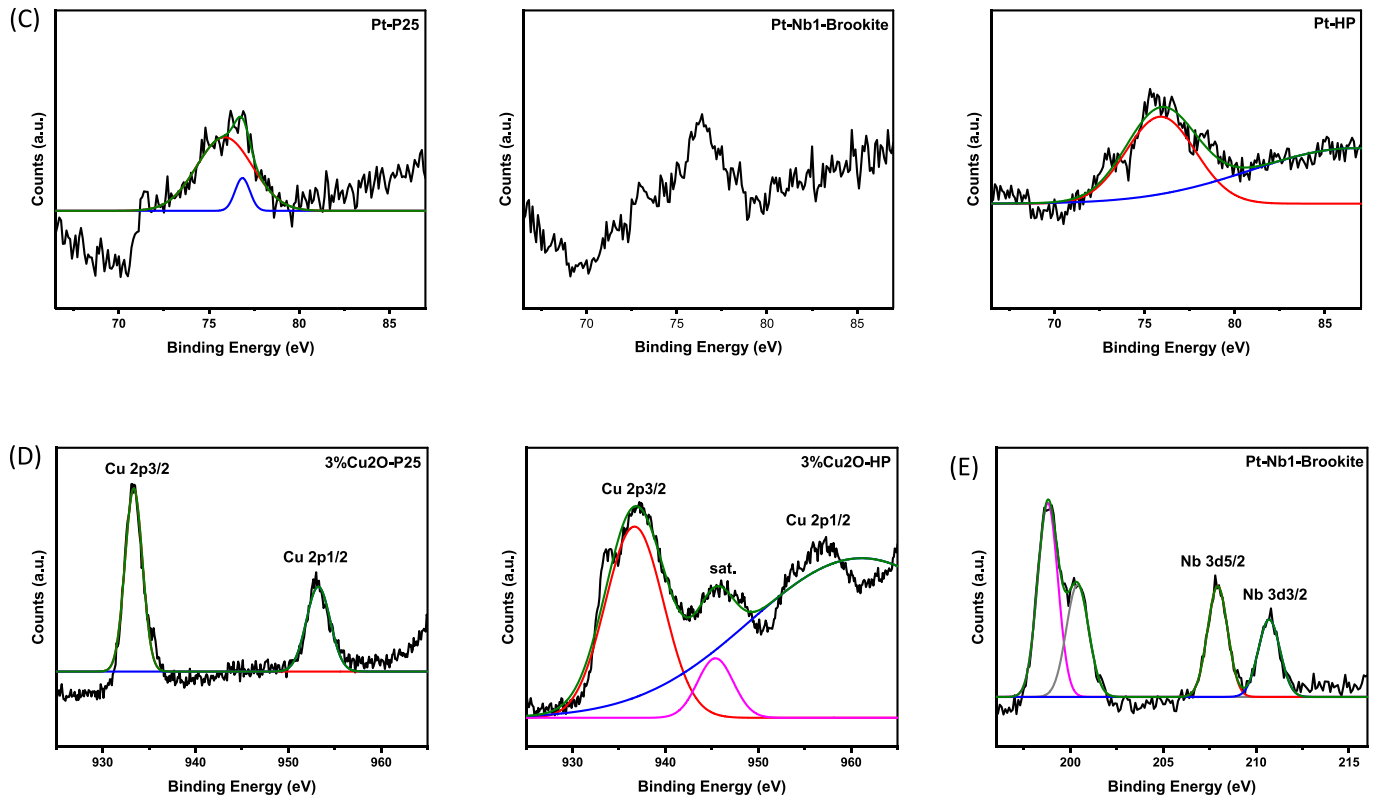

Fig. 5. (*continued*).

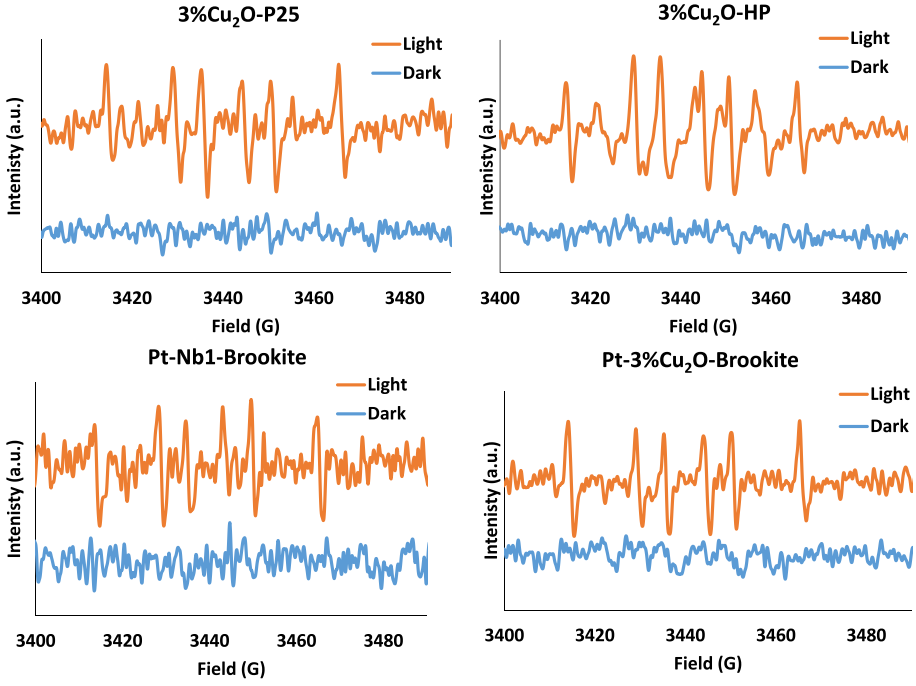

Fig. 6. EPR spectra of MeOH suspended samples in the presence of DMPO.

1604 and 1445 cm^{-1} observed in Fig. 8B and 8D for the spectra of Pt-BDH and Pt-Brookite samples could be due to electronic effects of Pt ensembles on the pyridine ring coordinated to Lewis acid sites on the surface.

In Table 1 are also reported the quantitative results related to pyridine TPD measurements in terms of amount and density of global acidic sites regardless of their nature (Brønsted and Lewis sites) present on the surface of different catalysts, and the corresponding temperatures of pyridine desorption. Pyridine TPD profiles are shown in Fig. S8. Comparing the pristine TiO_2 samples, Brookite and BDH solids display the highest and the lowest amount of acid sites, respectively; P25 sample shows less than half with respect to Brookite sample and HP solid has an

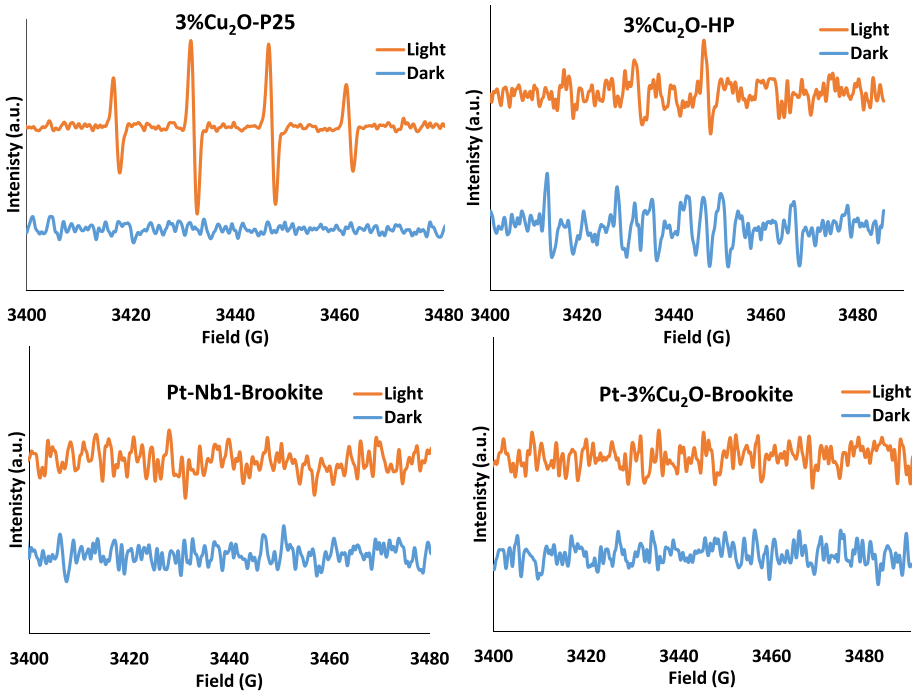

Fig. 7. EPR spectra of water suspended samples in the presence of DMPO and H_2O_2.

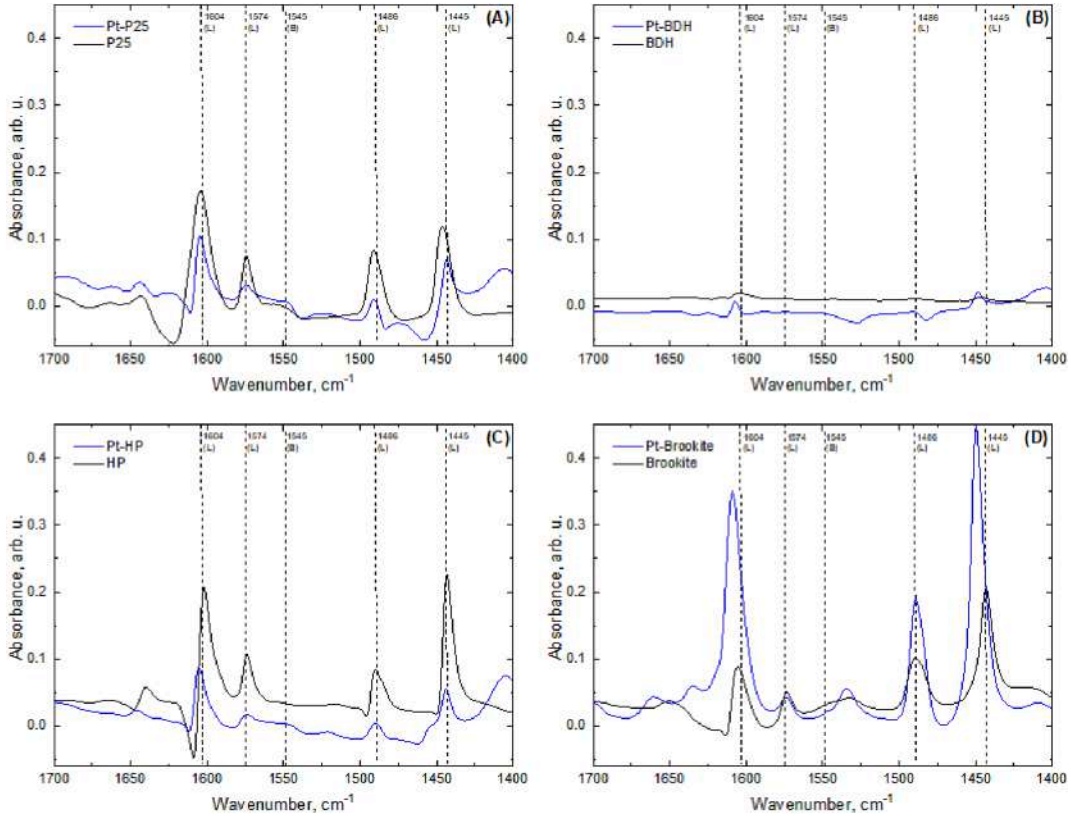

Fig. 8. DRIFTS spectra of pyridine adsorbed on the surface of investigated materials; (A) P25 based solids, (B) BDH based samples, (C) HP based materials, and (D) brookite based photocatalysts.

intermediate amount.

After Pt deposition one can notice a decrease of the quantity of acid sites in all the TiO_2 bare samples, except for Brookite solid, and the appearance of a second desorption peak except for HP sample. Moreover, a general increase in the temperature of pyridine desorption can be observed in the presence of Pt, which implies a rise in the acid strength of the sites. The coupling with Cu_2O commonly reduces the desorption temperature and has different effects on the quantity of acid

sites present on the various samples. In particular, it has a little effect on the amount of acid sites in P25 and HP samples, whilst a decrease is observed in Brookite solid. The latter is the only sample in which, in the presence of Cu_2O, the desorption temperature of the pyridine is practically equal to that of the bare sample. Moreover, a second desorption peak at higher temperature is visible. In the Pt-Nb1-Brookite sample, the addition of Nb reduces the amount of acid sites with respect to Pt-Brookite sample and has not influence on the temperature of pyridine desorption.

The TPD technique after CO_2 adsorption on TiO_2 surface allows to study the basic surface properties of the different catalysts. In Fig. 9 are shown the CO_2-TPD profiles of the investigated samples and in Table 2 are reported the amounts of basic sites. The peaks between 323 and 423 K are ascribed to the desorption of molecular CO_2, whilst those at higher temperatures to HCO_3^- or carboxylate deriving from the interaction of CO_2 with the TiO_2 surface hydroxyl groups [91]. The presence of peaks at higher temperatures indicates the existence of a stronger adsorption of CO_2 on the catalysts.

The observation of Table 2 related to pristine TiO_2 reveals that pure anatase (BDH sample) exhibits the least number of basic sites, the mixtures of anatase and rutile (P25 and HP solids) have the same middle amount, whilst brookite possesses the highest quantity. After the Pt addition, an increase, except for BDH sample, can be noted and Pt-P25 solid displays the largest amount of basic sites in the high temperature range.

3.1. Photocatalytic conversion of glucose and fructose

All TiO_2 based samples were compared for glucose and fructose aqueous photo-reforming under UV light irradiation in anaerobic conditions with the aim to link the reactivity to some catalyst's features. The photocatalytic results obtained with the two substrates are reported in Tables 3 and 4. Pt enhances the photoactivity thanks to its role in the reduction of the recombination rate (in accordance with the PL results) and it is essential for H_2 production, as only compounds deriving from the partial oxidation of the starting substrates and CO_2 originating from mineralization were observed in the presence of naked TiO_2 [60]. The main identified intermediates in the liquid phase deriving from the partial oxidation of the starting substrates are arabinose, erythrose, gluconic acid, glucaric acid, fructose (starting from glucose) and formic acid (Scheme 1), whereas H_2 and CO_2 are measured in the gaseous phase present in the head space of the photoreactor. In Fig. 10 are reported the concentration of glucose, fructose, the molecules obtained from their oxidation in liquid phase and those in the head space, CO_2 and H_2, versus irradiation time in the presence of the most active photocatalysts. All the samples give rise to the same compounds highlighting the same reaction mechanism (Scheme 1), but a different conversion degree, distribution of intermediates and H_2 production were observed with the different photocatalysts for both the substrates (Tables 3 and 4). The electronic and physico-chemical features of the different TiO_2 based materials, such as recombination rate of the photogenerated charges, polymorphic form, hydroxylation degree, crystallinity percentages, surface interactions between the catalysts and the substrates, surface acidity, are the causes of their different photocatalytic behaviours [26,60,92].

Starting from glucose as substrate, fructose is formed by isomerization, and both can form gluconic acid by the oxidation of the anomeric C_1 center converting the aldehydic group to the carboxylic one. All the catalysts give rise to low amounts of glucaric acid starting both from glucose and fructose. A parallel mechanism consists in the α-scission of the carbohydrates giving rise to arabinose in the first step and erythrose in the second one along to formic acid and hydrogen [60,93,94]. In our experiment, starting from glucose, arabinose is the main product and traces of erythrose are observed with some catalysts, whilst starting from fructose, erythrose is essentially formed, confirming the breaking of the chain at the carbon bonded to carbonyl.

Negligible amounts of H_2 are formed by using the pristine TiO_2 samples and the largely used Pt was essential to obtain satisfactory amounts. The coupling of TiO_2 with Cu_2O is beneficial both for conversion and selectivity for P25 sample, whilst it exhibits a slightly negative effect on Brookite and HP solids, in any cases was effective in replacing Pt for H_2 formation, avoiding the use of noble metal species.

Home prepared samples were competitive with the commercial ones being more active than the benchmark P25 solid. The commercial samples afford less photocatalytic conversion for glucose and fructose than the home prepared ones. The highest glucose conversion (40 %) is obtained with Pt-HP samples, whilst the most oxidant sample for fructose is Pt-Nb1-Brookite (conversion 50 %). With the sample Pt-HP, almost the same degree of conversion is reached with the two substrates, while for fructose lower selectivity values but greater quantities of H_2 compared to glucose are obtained.

With glucose Pt-Brookite based samples show a little increase in the conversion, a generally decrease in selectivity towards fructose and an enhanced H_2 formation. By using Pt-Brookite and Pt-Nb1-Brookite samples, the conversion of glucose is similar, the Nb addition slightly enhances the selectivity towards the intermediates and fructose is also formed, but H_2 formation is somewhat lower than that obtained with Pt-Brookite. The slight high oxidant power of the samples containing Nb could be due to the formation of an effective heterojunction between TiO_2 and Nb_2O_5 in accordance with Azevedo-Rafael et al [95]. HP based powders exhibit the highest conversion percentages and selectivity towards arabinose. To investigate the role of hydroxyl radicals in the formation of the different compounds, runs in the presence of *tert*-butanol, used as hydroxyl radicals scavenger, were carried out in the presence of two photocatalysts: Pt-HP that afforded the highest glucose conversion and selectivity towards arabinose, and Pt-BDH which did not produce arabinose. The obtained results are reported in the Table S3. In both cases a decrease in the conversion can be noticed although the effect is more evident for Pt-BDH. This means that hydroxyl radicals have a more pronounced role towards the conversion of glucose in the

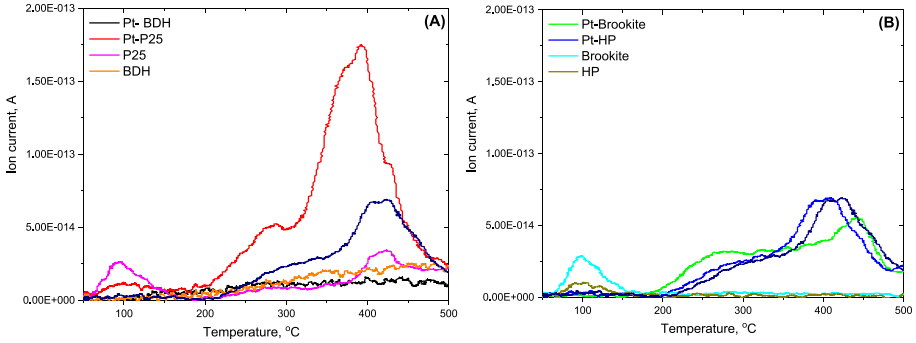

Fig. 9. CO_2 TPD profiles of investigated materials.

Table 2
Amount and density of basic sites on the surface of investigated materials determined by TPD in the presence of CO_2.

Sample	Mass of catalyst (g)	Peak area (A s)	Amount of basic sites (μmol/g)	Density of basic sites (μmol/m^2)
BDH	0.0447	$2.95 \cdot 10^{-11}$	8.14	0.814
Pt-BDH	0.0521	$2.09 \cdot 10^{-11}$	8.05	0.805
P25	0.0507	$3.69 \cdot 10^{-11}$	12.1	0.242
Pt-P25	0.0518	$1.29 \cdot 10^{-10}$	81.7	1.634
Brookite	0.0518	$1.85 \cdot 10^{-11}$	28.3	0.288
Pt-Brookite	0.0502	$5.75 \cdot 10^{-11}$	74.7	0.762
HP	0.0499	$7.38 \cdot 10^{-12}$	12.8	0.164
Pt-HP	0.0520	$5.74 \cdot 10^{-11}$	53.6	0.687

Table 3
Glucose conversion, selectivity towards fructose, gluconic acid, arabinose and formic acid, and H_2 and CO_2 production. The listed values were obtained after 5 h of irradiation.

Photocatalyst	Conversion (%)	Selectivity (%)				H_2 [mM]	CO_2 [mM]
		Fructose	Gluconic acid	Arabinose	Formic acid		
P25	12	22	1.5	38	29	–	0.03
Pt-P25	32	31	4.6	41	31	1.93	0.07
3 %Cu_2O-P25	28	19	8.0	30	32	1.25	0.06
Pt-BDH	21	58	4.9	–	13	1.44	0.03
Pt-Brookite	33	–	2.5	27	40	2.71	0.09
Pt-Nb1-Brookite	35	12	3.7	32	31	2.40	0.09
3 %Cu_2O-Brookite	26	20	3.0	36	25	1.20	0.08
Pt-3 %Cu_2O-Brookite	30	–	3.1	37	34	2.03	0.08
Pt-HP	40	27	2.6	45	44	1.89	0.14
3 %Cu_2O-HP	37	–	3.0	49	37	1.51	0.07

Table 4
Fructose conversion, selectivity towards gluconic acid, formic acid, erythrose, and H_2 and CO_2 production. The listed values were obtained after 5 h of irradiation.

Photocatalyst	Conversion (%)	Selectivity (%)			H_2 [mM]	CO_2 [mM]
		Gluconic acid	Formic acid	Erythrose		
Pt-P25	25	9.0	12	–	3.13	0.11
3 %Cu_2O-P25	35	5.0	5	–	1.80	0.08
Pt-BDH	28	4.1	7	–	1.34	0.02
Pt-Brookite	42	2.7	12	3.80	3.20	0.12
Pt-Nb1-Brookite	50	2.0	11	2.68	3.16	0.11
3 %Cu_2O-Brookite	32	2.2	11	–	1.65	0.09
Pt-3 %Cu_2O-Brookite	35	0.5	25	5.27	2.55	0.09
Pt-HP	40	4.5	6	7.47	3.26	0.12
3 %Cu_2O-HP	35	6.2	17	7.60	1.70	0.09

presence of Pt-BDH. Also, the selectivity towards arabinose (formed only in the presence of Pt-HP) decreases after adding *tert*-butanol highlighting that hydroxyl radicals influence the formation of this compound, but they are not the only active species. Quantum efficiency of the sample Pt-HP, calculated following the method reported in ref. [26], is 0.01 %.

The maximum hydrogen concentration is obtained with the Pt-Brookite photocatalyst that displays the highest amount of acidic cites. Among the Pt-containing samples, Pt-BDH exhibits the lowest glucose conversion and formic acid selectivity, the highest fructose selectivity and no arabinose formation indicating a different reaction pathway [60,94]. This finding is different from the results of Román-Leshkov et al. [96] who attributed the catalytic isomerization of glucose to fructose by using tin-containing zeolite Sn-Beta as catalyst to the presence of Lewis acidic sites. In our case the solid with the lowest number of acidic sites (Table 1 and DRIFTS measurements) gives rise to the highest fructose formation. Probably, other features as catalyst type (we use TiO_2 instead of zeolite-based catalyst), preparation method, and reaction temperature play a fundamental role. Considering that there is not a monotonic trend between photoactivity and surface acidity/basicity and that the used samples differ not only in surface acidity/basicity, it is difficult to establish the mechanism by which these properties influence activity/selectivity. This is an aspect investigated in the literature and for which a clear answer has not yet been found. In some conditions it has been found that catalysts with Lewis (LA) and/or Brønsted acid (BA) sites are needed for sugar conversions, however there is no agreement among researchers which type and strength of acidic sites are required [68,97]. Interestingly, Abdouli et al. [97] compared the performance of TiO_2 samples towards glucose conversion by a catalytic and a photocatalytic approach. They found that while the photocatalytic performances could be linked to the catalysts' Lewis acid sites density and their glucose adsorption capacities, the hydrothermal performances were dependent of the catalysts' basic/acid sites balance.

The different reactivity of similar organic compounds (including isomers) is well known in the literature [26,92]. By using fructose as substrate, a generally higher conversion and lower selectivity towards the partial oxidation compounds is obtained with respect to glucose. A tentative explanation can be the following: in aqueous solution glucose is essentially present in the pyranose form while fructose in the furanose one. It is well known that the furanose rings are thermodynamically less stable than the pyranose ones, and this could explain the generally higher conversion of fructose with respect to glucose observed in our experiments. Notably, for both the substrates, the most efficient catalysts are Pt-Brookite and Pt-Nb1-Brookite both for conversion and production of H_2, in accordance with previous results [59,60,80]. Pt-Brookite revealed the best performance towards H_2 evolution from

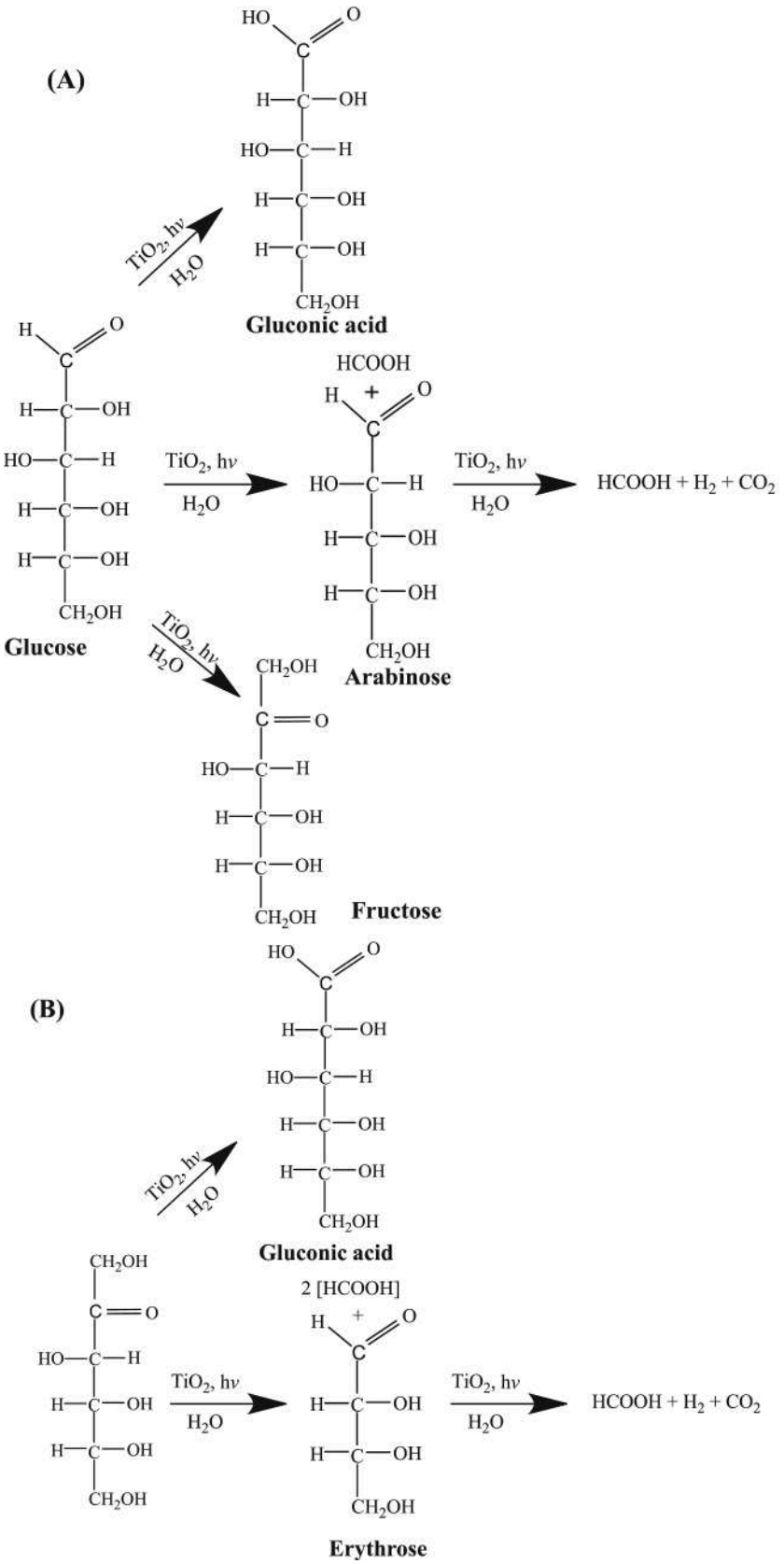

Scheme 1. Hypothesized reaction mechanism of photo-reforming of (A) glucose and (B) fructose.

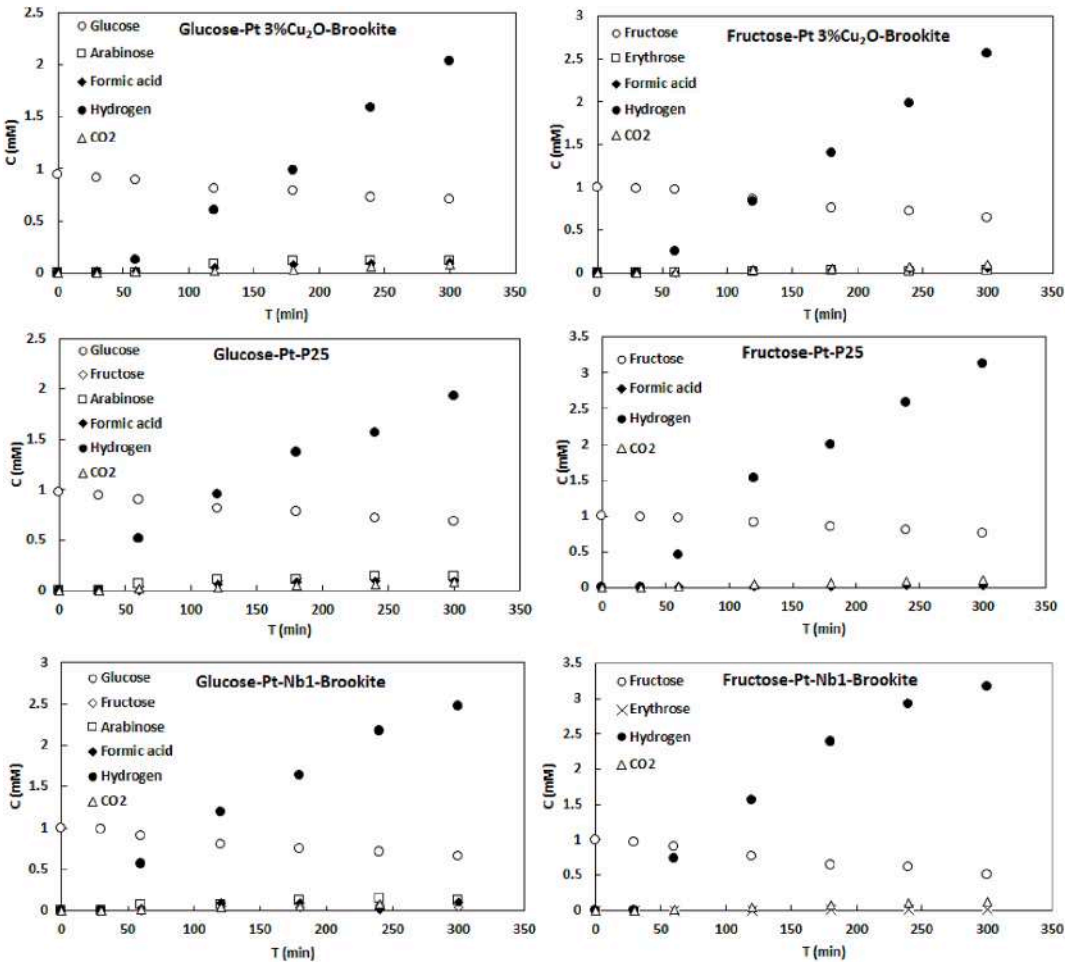

Fig. 10. Concentration of (○) glucose, (◊) fructose, (□) arabinose, (x) erythrose, (◆) formic acid, (●) H_2, and (Δ) CO_2 versus irradiation time in the presence of various photocatalysts after 5 h of irradiation.

aqueous solution containing glycerol [80]. An *in situ* FT-IR study showed the highest ability of this polymorph to adsorb water.

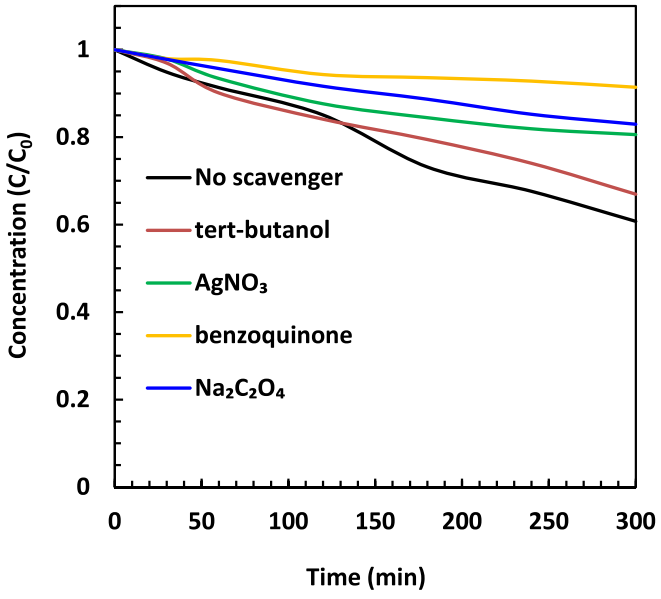

Fig. 11. Comparison of the glucose degradation in the presence of different scavengers.

The obtained results highlight the peculiar role of the interactions between the substrates and the surface of a specific photocatalyst [26]. Moreover, although the performance is not excellent, some of the prepared samples showed a photoactivity comparable with that of other TiO_2 based photocatalysts (see Table S4), both with regards to the production of H_2 and towards the formation of high value products deriving from glucose. Notably, it should also be considered that in some papers only the formation of H_2 is reported while in others only the reaction intermediates.

The results obtained with glucose in the presence of the different scavengers and Pt-HP as photocatalyst are reported in the Fig. 11. By adding *tert*-butanol a slight decrease in the glucose conversion is obtained revealing a marginal role of $^{\bullet}OH$ radicals whilst a remarkable reduction is observed in the presence of the other scavengers highlighting the important role played by e^-, h^+ and principally by $^{\bullet}O_2^-$ species.

4. Conclusions

In conclusion, the activity of various commercial and home prepared modified TiO_2 photocatalysts was compared for the photo-reforming of two biomass derivatives (glucose and fructose) selected as probe molecules. Numerous structural and surface characterizations have highlighted the different properties of the used samples and some of them have been related to the photocatalytic activity, although a direct correlation to a specific property was not found. This confirms the dependence of photoactivity on a number of parameters. Importantly, the

home-prepared catalysts are more active than the commercial catalysts both in hydrogen generation and in the formation of partial oxidation compounds being Pt-Brookite the most active sample for H_2 production and Pt-HP the best for partial oxidation of both glucose and fructose. The role of Pt in modifying the basic surface properties of the different TiO_2 based photocatalysts has been highlighted whilst a direct correlation between surface acidity/basicity and photocatalytic activity was not found due to the heterogeneity of the samples.

CRediT authorship contribution statement

Muhammad Umair: Investigation. **Vittorio Loddo:** Data curation, Visualization. **Leonardo Palmisano:** Supervision, Writing – review & editing. **Albin Pintar:** Data curation, Investigation. **Gregor Žerjav:** Investigation, Data curation. **Giovanni Palmisano:** Visualization, Investigation, Data curation. **Samar Al Jitan:** Investigation, Data curation. **Marianna Bellardita:** Writing – review & editing, Writing – original draft, Supervision, Data curation, Conceptualization.

Declaration of competing interest

The authors declare that they have no known competing financial interests or personal relationships that could have appeared to influence the work reported in this paper.

Data availability

No data was used for the research described in the article.

Acknowledgement

Dr. Thomas Delclos is gratefully acknowledged for XPS analysis. Eng. Reem Al Sakkaf is thankfully recognized for SEM analysis.

Appendix A. Supplementary data

Supplementary data to this article can be found online at https://doi.org/10.1016/j.jphotochem.2024.115654.

References

[1] I. Dincer, Renew. Sustain. Energy Rev. 4 (2) (2000) 157–175, https://doi.org/10.1016/S1364-0321(99)00011-8.
[2] T.G. Ambaye, M. Vaccari, A. Bonilla-Petriciolet, S. Prasad, E.D. van Hullebusch, S. Rtimi, J. Environ. Manage. 290 (2021) 112627, https://doi.org/10.1016/J.JENVMAN.2021.112627.
[3] M. Bellardita, V. Loddo, L. Palmisano, Mini Rev Org Chem 17 (7) (2020) 884–901, https://doi.org/10.2174/1570193x17666200131112856.
[4] J.C. Serrano-Ruiz, R. Luque, A. Sepúlveda-Escribano, Chem. Soc. Rev. 40 (11) (2011) 5266–5281, https://doi.org/10.1039/C1CS15131B.
[5] R. Ahorsu, F. Medina, M. Constantí, Energies 11 (2018) 12, https://doi.org/10.3390/EN11123366.
[6] J. Tomaszewska, D. Bieliński, M. Binczarski, J. Berlowska, P. Dziugan, J. Piotrowski, A. Stanishevsky, I.A. Witońska, RSC Adv. 8 (6) (2018) 3161–3177, https://doi.org/10.1039/c7ra12782k.
[7] M. Ventura, A. Marinas, M.E. Domine, Top. Catal. 63 (9–10) (2020) 846–865, https://doi.org/10.1007/s11244-020-01309-9.
[8] C.H. Zhou, X. Xia, C.X. Lin, D.S. Tong, J. Beltramini, Chem. Soc. Rev. 40 (11) (2011) 5588–5617, https://doi.org/10.1039/c1cs15124j.
[9] Z. Abdin, A. Zafaranloo, A. Rafiee, W. Mérida, W. Lipiński, K.R. Khalilpour, Renew. Sustain. Energy Rev. 120 (2020), https://doi.org/10.1016/J.RSER.2019.109620.
[10] P.J. Megia, A.J. Vizcaino, J.A. Calles, A. Carrero, Energy Fuel 35 (20) (2021) 16403–16415, https://doi.org/10.1021/ACS.ENERGYFUELS.1C02501.
[11] F. Qureshi, M. Yusuf, H. Kamyab, D.V.N. Vo, S. Chelliapan, S.W. Joo, Y. Vasseghian, Renew. Sustain. Energy Rev. 168 (2022) 112916, https://doi.org/10.1016/J.RSER.2022.112916.
[12] J. Esteban, P. Yustos, M. Ladero, Catalysts (2018), https://doi.org/10.3390/catal8120637.
[13] X. Liu, X. Duan, W. Wei, S. Wang, B.J. Ni, Green Chem. (2019) 4266–4289, https://doi.org/10.1039/c9gc01728c.
[14] F. Guo, Z. Fang, T.J. Zhou, Bioresour. Technol. 112 (2012) 313–318, https://doi.org/10.1016/J.BIORTECH.2012.02.108.
[15] G.C. de Assis, I.M.A. Silva, T.G. dos Santos, T.V. dos Santos, M.R. Meneghetti, S.M. P. Meneghetti, Cat. Sci. Technol. (2021) 2354–2360, https://doi.org/10.1039/d0cy02358b.
[16] B. Ma, Y. Wang, X. Guo, X. Tong, C. Liu, Y. Wang, X. Guo, Appl. Catal. A 552 (2018) 70–76, https://doi.org/10.1016/J.APCATA.2018.01.002.
[17] Y. Zhang, S. Yang, Z. Wang, H. Qin, G. Lyu, J. Chen, G. Yang, J. Catal. 413 (2022) 843–857, https://doi.org/10.1016/J.JCAT.2022.07.042.
[18] M. Bellardita, E.I. García-López, G. Marcì, B. Megna, F.R. Pomilla, L. Palmisano, RSC Adv. 5 (73) (2015) 59037–59047, https://doi.org/10.1039/c5ra09894g.
[19] M. Bellardita, E.I. García-López, G. Marcì, G. Nasillo, L. Palmisano, Eur. J. Inorg. Chem. 2018 (41) (2018) 4522–4532, https://doi.org/10.1002/EJIC.201800663.
[20] U.I. Gaya, A.H. Abdullah, J Photochem Photobiol C: Photochem Rev (2008) 1–12, https://doi.org/10.1016/j.jphotochemrev.2007.12.003.
[21] D. Friedmann, A. Hakki, H. Kim, W. Choi, D. Bahnemann, Green Chem. (2016) 5391–5411, https://doi.org/10.1039/c6gc01582d.
[22] F. Parrino, M. Bellardita, E.I. García-López, G. Marcì, V. Loddo, L. Palmisano, ACS Catal. 8 (12) (2018) 11191–11225, https://doi.org/10.1021/acscatal.8b03093.
[23] L. Palmisano, V. Augugliaro, M. Bellardita, A. Di Paola, E. García López, V. Loddo, G. Marcì, G. Palmisano, S. Yurdakal, ChemSusChem (2011) 1431–1438, https://doi.org/10.1002/cssc.201100196.
[24] A. Shokri, M. Sanavi Fard, Chem. Pap. (2022) 5309–5339, https://doi.org/10.1007/s11696-022-02256-3.
[25] W.S. Koe, J.W. Lee, W.C. Chong, Y.L. Pang, L.C. Sim, Environ. Sci. Pollut. Res. (2020) 2522–2565, https://doi.org/10.1007/s11356-019-07193-5.
[26] M. Bellardita, M. Feilizadeh, R. Fiorenza, S. Scirè, L. Palmisano, V. Loddo, Photochem. Photobiol. Sci. (2022), https://doi.org/10.1007/s43630-022-00284-2.
[27] K. Nakata, A. Fujishima, J Photochem Photobiol C: Photochem Rev (2012) 169–189, https://doi.org/10.1016/j.jphotochemrev.2012.06.001.
[28] K. Hashimoto, H. Irie, A. Fujishima, J. Ind. Eng. Chem. 44 (12) (2005) 8269–8285, https://doi.org/10.1143/JJAP.44.8269.
[29] H. Dong, G. Zeng, L. Tang, C. Fan, C. Zhang, X. He, Y. He, Water Res. (2015) 128–146, https://doi.org/10.1016/j.watres.2015.04.038.
[30] I. Arora, H. Chawla, A. Chandra, S. Sagadevan, S. Garg, Inorg. Chem. Commun. 143 (2022) 109700, https://doi.org/10.1016/J.INOCHE.2022.109700.
[31] H. Tyagi, H. Chawla, H. Bhandari, S. Garg, Mater. Today:. Proc. 49 (2020) 3289–3305, https://doi.org/10.1016/J.MATPR.2020.12.1036.
[32] R. Fiorenza, S. Sciré, L. D'Urso, G. Compagnini, M. Bellardita, L. Palmisano, Int. J. Hydrogen Energy 44 (29) (2019) 14796–14807, https://doi.org/10.1016/j.ijhydene.2019.04.035.
[33] M. Bellardita, H.A.E. Nazer, V. Loddo, F. Parrino, A.M. Venezia, L. Palmisano, Catal. Today 284 (2017) 92–99, https://doi.org/10.1016/j.cattod.2016.11.026.
[34] P.A. Osorio-Vargas, C. Pulgarin, A. Sienkiewicz, L.R. Pizzio, M.N. Blanco, R. A. Torres-Palma, C. Pétrier, J.A. Rengifo-Herrera, Ultrason. Sonochem. 19 (3) (2012) 383–386, https://doi.org/10.1016/j.ultsonch.2011.11.013.
[35] A.M. Djaballah, M. Bellardita, L. Palmisano, V. Loddo, M. Umair, C.M. Pecoraro, R. Bagtache, M. Trari, Mol. Catal. 546 (2023) 113251, https://doi.org/10.1016/j.mcat.2023.113251.
[36] C.M. Pecoraro, M. Bellardita, V. Loddo, F. Di Franco, L. Palmisano, M. Santamaria, J. Ind. Eng. Chem. 118 (2023) 247–258, https://doi.org/10.1016/j.jiec.2022.11.010.
[37] J. Low, J. Yu, M. Jaroniec, S. Wageh, A.A. Al-Ghamdi, Adv. Mater. (2017), https://doi.org/10.1002/adma.201601694.
[38] J. Duan, H. Zhao, Z. Zhang, W. Wang, Ceram. Int. 44 (18) (2018) 22748–22759, https://doi.org/10.1016/j.ceramint.2018.09.062.
[39] A. Di Paola, S. Ikeda, G. Marcì, B. Ohtani, L. Palmisano, Int. J. Photoen. 3 (2001) 370924, https://doi.org/10.1155/S1110662X01000216.
[40] X. Sun, H. Liu, J. Dong, J. Wei, Y. Zhang, Catal Letters 135 (3–4) (2010) 219–225, https://doi.org/10.1007/s10562-010-0302-7.
[41] B. Choudhury, B. Borah, A. Choudhury, Photochem. Photobiol. 88 (2) (2012) 257–264, https://doi.org/10.1111/j.1751-1097.2011.01064.x.
[42] S. Ikeda, N. Sugiyama, B. Pal, G. Marcí, L. Palmisano, H. Noguchi, K. Uosaki, B. Ohtani, PCCP 3 (2) (2001) 267–273, https://doi.org/10.1039/b008028o.
[43] O. Fontelles-Carceller, M.J. Muñoz-Batista, J.C. Conesa, M. Fernández-García, A. Kubacka, Appl Catal B 216 (2017) 133–145, https://doi.org/10.1016/J.APCATB.2017.05.022.
[44] T. Ohno, M. Akiyoshi, T. Umebayashi, K. Asai, T. Mitsui, M. Matsumura, Appl. Catal. A 265 (1) (2004) 115–121, https://doi.org/10.1016/J.APCATA.2004.01.007.
[45] R. Fiorenza, M. Bellardita, S. Scirè, L. Palmisano, Mol. Catal. 455 (2018) 108–120, https://doi.org/10.1016/j.mcat.2018.06.002.
[46] M. Díaz-Sánchez, R.N. Murgu, D. Díaz-García, J.M. Méndez-Arriaga, S. Prashar, B. Urbán, J. Pinkas, M. Lamač, M. Horáček, S. Gómez-Ruiz, Adv Sustain Syst 5 (2021) 11, https://doi.org/10.1002/adsu.202000298.
[47] J. Ortiz-Bustos, S. Gómez-Ruiz, J. Mazarío, M.E. Domine, I. Del Hierro, Y. Pérez, Cat. Sci. Technol. 10 (19) (2020) 6511–6524, https://doi.org/10.1039/d0cy01041c.
[48] F. Boccuzzi, A. Chiorino, G. Martra, M. Gargano, N. Ravasio, B. Carrozzini, J. Catal. 165 (1997) 129–139, https://doi.org/10.1006/jcat.1997.1475.
[49] C.K. Nuo Peh, X.-Q. Wang, G.W. Ho, Procedia Eng 215 (2017) 171–179, https://doi.org/10.1016/j.proeng.2017.11.006.
[50] Y.H. Zhang, M.M. Liu, J.L. Chen, K.F. Xie, S.M. Fang, J. Phys. Chem. Solid 152 (2021), https://doi.org/10.1016/j.jpcs.2021.109948.
[51] M.E. Aguirre, R. Zhou, A.J. Eugene, M.I. Guzman, M.A. Grela, Appl Catal B 217 (2017) 485–493, https://doi.org/10.1016/j.apcatb.2017.05.058.
[52] M. Muscetta, R. Andreozzi, L. Clarizia, I. di Somma, R. Marotta, Int. J. Hydrogen Energy (2020) 28531–28552, https://doi.org/10.1016/j.ijhydene.2020.07.225.

[53] M.O. Segovia-Guzmán, M. Román-Aguirre, J.Y. Verde-Gomez, V.H. Collins-Martínez, G. Zaragoza-Galán, V.H. Ramos-Sánchez, Catal. Today 349 (2020) 88–97, https://doi.org/10.1016/j.cattod.2018.05.031.
[54] A. Di Paola, M. Bellardita, L. Palmisano, Catalysts (2013) 36–73, https://doi.org/10.3390/catal3010036.
[55] A. Di Paola, G. Cufalo, M. Addamo, M. Bellardita, R. Campostrini, M. Ischia, R. Ceccato, L. Palmisano, Colloids Surf A Physicochem Eng Asp 317 (1–3) (2008) 366–376, https://doi.org/10.1016/j.colsurfa.2007.11.005.
[56] L. Liu, H. Zhao, J.M. Andino, Y. Li, ACS Catal. 2 (8) (2012) 1817–1828, https://doi.org/10.1021/cs300273q.
[57] Z. Li, S. Cong, Y. Xu, ACS Catal. 4 (9) (2014) 3273–3280, https://doi.org/10.1021/cs500785z.
[58] G. Zerjav, K. Zizek, J. Zavasnik, A. Pintar, J. Environ. Chem. Eng. 10 (2022) 3, https://doi.org/10.1016/j.jece.2022.107722.
[59] E. Wierzbicka, M. Altomare, M. Wu, N. Liu, T. Yokosawa, D. Fehn, S. Qin, K. Meyer, T. Unruh, E. Spiecker, L. Palmisano, M. Bellardita, J. Will, P. Schmuki, J. Mater. Chem. A 9 (2) (2021) 1168–1179, https://doi.org/10.1039/d0ta09066b.
[60] M. Bellardita, E.I. García-López, G. Marcì, L. Palmisano, Int. J. Hydrogen Energy 41 (14) (2016) 5934–5947, https://doi.org/10.1016/j.ijhydene.2016.02.103.
[61] M.V. Dozzi, G.L. Chiarello, M. Pedroni, S. Livraghi, E. Giamello, E. Selli, Appl Catal B 209 (2017) 417–428, https://doi.org/10.1016/j.apcatb.2017.03.007.
[62] J. Yu, L. Qi, M. Jaroniec, J. Phys. Chem. C 114 (30) (2010) 13118–13125, https://doi.org/10.1021/jp104488b.
[63] M. Muscetta, S. Al Jitan, G. Palmisano, R. Andreozzi, R. Marotta, S. Cimino, I. Di Somma, J. Environ. Chem. Eng. 10 (3) (2022), https://doi.org/10.1016/j.jece.2022.107735.
[64] Y. Li, B. Wang, S. Liu, X. Duan, Z. Hu, Appl. Surf. Sci. 324 (2015) 736–744, https://doi.org/10.1016/j.apsusc.2014.11.027.
[65] L. Cheng, B. Li, H. Yin, J. Fan, Q. Xiang, J. Mater. Sci. Technol. 118 (2022) 54–63, https://doi.org/10.1016/j.jmst.2021.11.055.
[66] L. Cheng, P. Zhang, Q. Wen, J. Fan, Q. Xiang, Chin. J. Catal. 43 (2) (2022) 451–460, https://doi.org/10.1016/S1872-2067(21)63879-2.
[67] M.V. Nogueira, G.M.M.M. Lustosa, Y. Kobayakawa, W. Kogler, M. Ruiz, E. S. Monteiro Filho, M.A. Zaghete, L.A. Perazolli, Adv. Mater. Sci. Eng. 2018 (2018), https://doi.org/10.1155/2018/7326240.
[68] H.T. Kreissl, K. Nakagawa, Y.K. Peng, Y. Koito, J. Zheng, S.C.E. Tsang, J. Catal. 338 (2016) 329–339, https://doi.org/10.1016/j.jcat.2016.03.007.
[69] H. Zhang, J.F. Banfield, J. Phys. Chem. B 104 (15) (2000) 3481–3487, https://doi.org/10.1021/jp000499j.
[70] M. Bellardita, A. Di Paola, B. Megna, L. Palmisano, J. Photochem. Photobiol. A Chem. 367 (2018) 312–320, https://doi.org/10.1016/j.jphotochem.2018.08.042.
[71] M. Bellardita, A. Di Paola, B. Megna, L. Palmisano, Appl Catal B 201 (2017) 150–158, https://doi.org/10.1016/j.apcatb.2016.08.012.
[72] D. Maučec, A. Šuligoj, A. Ristić, G. Dražić, A. Pintar, N.N. Tušar, Catal. Today 310 (2018) 32–41, https://doi.org/10.1016/j.cattod.2017.05.061.
[73] V. Etacheri, C. Di Valentin, J. Schneider, D. Bahnemann, S.C. Pillai, J Photochem Photobiol C: Photochem Rev 25 (2015) 1–29, https://doi.org/10.1016/J.JPHOTOCHEMREV.2015.08.003.
[74] A. Takai, P.V. Kamat, ACS Nano 5 (9) (2011) 7369–7376, https://doi.org/10.1021/nn202294b.
[75] S. Al Jitan, Y. Li, D. Bahamon, G. Žerjav, V.S. Tatiparthi, C. Aubry, M. Sinnokrot, Z. Matouk, N. Rajput, M. Gutierrez, K. Al-Ali, R. Hashaikeh, A. Pintar, L.F. Vega, G. Palmisano, J. Environ. Chem. Eng. 11 (2) (2023), https://doi.org/10.1016/j.jece.2023.109485.
[76] N.D. Abazović, M.I. Čomor, M.D. Dramićanin, D.J. Jovanović, S.P. Ahrenkiel, J. M. Nedeljković, J. Phys. Chem. B 110 (50) (2006) 25366–25370, https://doi.org/10.1021/jp064454f.
[77] F. Xu, W. Xiao, B. Cheng, J. Yu, Int. J. Hydrogen Energy 39 (28) (2014) 15394–15402, https://doi.org/10.1016/j.ijhydene.2014.07.166.
[78] M. Bellardita, V. Augugliaro, V. Loddo, B. Megna, G. Palmisano, L. Palmisano, M. A. Puma, Appl. Catal. A 441–442 (2012) 79–89, https://doi.org/10.1016/j.apcata.2012.07.019.
[79] M. Bellardita, A. Di Paola, L. Palmisano, F. Parrino, G. Buscarino, R. Amadelli, Appl Catal B 104 (3–4) (2011) 291–299, https://doi.org/10.1016/j.apcatb.2011.03.016.
[80] C.M. Pecoraro, L. Mino, E. Kozyr, L. Palmisano, F. di Franco, V. Loddo, M. Santamaria, M. Bellardita, Chem. Comm. 60 (2024) 3782–3785, https://doi.org/10.1039/D4CC00353E.
[81] T. Jedsukontorn, T. Ueno, N. Saito, M. Hunsom, J. Alloy. Compd. 726 (2017) 567–577, https://doi.org/10.1016/j.jallcom.2017.08.028.
[82] M. Bellardita, C. Garlisi, A.M. Venezia, G. Palmisano, L. Palmisano, Cat. Sci. Technol. 8 (6) (2018) 1606–1620, https://doi.org/10.1039/c7cy02382k.
[83] J.J. Murcia, M.C. Hidalgo, J.A. Navío, V. Vaiano, P. Ciambelli, D. Sannino, Int. J. Photoenerg 2012 (2012), https://doi.org/10.1155/2012/687262.
[84] J. Yan, G. Wu, N. Guan, L. Li, Appl Catal B 152–153 (1) (2014) 280–288, https://doi.org/10.1016/j.apcatb.2014.01.049.
[85] J. Huo, Y. Hu, H. Jiang, C. Li, Nanoscale 6 (15) (2014) 9078–9084, https://doi.org/10.1039/c4nr00972j.
[86] S. Songtawee, B. Rungtaweevoranit, C. Klaysom, K. Faungnawakij, RSC Adv. 11 (47) (2021) 29196–29206, https://doi.org/10.1039/d1ra06002c.
[87] V.V. Kumar, G. Naresh, S. Deepa, P.G. Bhavani, M. Nagaraju, M. Sudhakar, K.V. R. Chary, A. Venugopal, J. Tardio, S.K. Bhargava, Appl. Catal. A 531 (2017) 169–176, https://doi.org/10.1016/J.APCATA.2016.10.032.
[88] M. Addamo, M. Del Arco, M. Bellardita, D. Carriazo, A. Di Paola, E. García-López, G. Marcì, C. Martín, L. Palmisano, V. Rives, Res. Chem. Intermed. 33 (2007) 465–479, https://doi.org/10.1163/156856707779238685.
[89] M.I. Zaki, M.A. Hasan, F.A. Al-Sagheer, L. Pasupulety, Colloids Surf A Physicochem Eng Asp 190 (3) (2001) 261–274, https://doi.org/10.1016/S0927-7757(01)00690-2.
[90] L. Ding, M. Li, Y. Zhao, H. Zhang, J. Shang, J. Zhong, H. Sheng, C. Chen, J. Zhao, Appl Catal B 266 (2020), https://doi.org/10.1016/j.apcatb.2020.118634.
[91] J. Zhao, Y. Wang, Y. Li, X. Yue, C. Wang, Cat. Sci. Technol. 6 (22) (2016) 7967–7975, https://doi.org/10.1039/c6cy01365a.
[92] M. Bellardita, G. Escolano-Casado, L. Palmisano, L. Mino, Catal. Today (2022), https://doi.org/10.1016/j.cattod.2022.12.014.
[93] J.C. Colmenares, A. Magdziarz, A. Bielejewska, Bioresour. Technol. 102 (24) (2011) 11254–11257, https://doi.org/10.1016/j.biortech.2011.09.101.
[94] R. Chong, J. Li, Y. Ma, B. Zhang, H. Han, C. Li, J. Catal. 314 (2014) 101–108, https://doi.org/10.1016/j.jcat.2014.03.009.
[95] R.A. Rafael, F.B. Noronha, A.B. Gaspar, Top. Catal. 63 (11–14) (2020) 1066–1076, https://doi.org/10.1007/s11244-020-01313-z.
[96] Y. Román-Leshkov, M. Moliner, J.A. Labinger, M.E. Davis, Angewandte Chemie - International Edition 49 (47) (2010) 8954–8957, https://doi.org/10.1002/anie.201004689.
[97] I. Abdouli, M. Eternot, F. Dappozze, C. Guillard, N. Essayem, Catal. Today 367 (2021) 268–277, https://doi.org/10.1016/j.cattod.2020.03.040.